Lauri Riuttanen

Thermal Annealing of AlN Thin Films Fabricated by Plasma-Enhanced Atomic Layer Deposition for GaN Epitaxy

Faculty of Electronics, Communications and Automation

Thesis submitted for examination for the degree of Master of Science in Technology.

Espoo 1.11.2010

Thesis supervisor:

Prof. Markku Sopanen

Thesis instructor:

D.Sc. (Tech.) Sami Suihkonen

Aalto University
School of Science
and Technology

Tekijä: Lauri Riuttanen	
Työn nimi: Plasma-avusteisella atomikerrosvalmistusmenetelmällä valmistetun alumiininitridikalvon lämpökäsittely ja soveltuvuus epitaktisen galliumnitridin alustana	
Päivämäärä: 1.11.2010 Kieli: Englanti	Sivumäärä:7+55

Elektroniikan, tietoliikenteen ja automaation tiedekunta

Mikro- ja nanotekniikan laitos

Professuuri: Optoelektroniikka   Koodi: S-104

Valvoja: Prof. Markku Sopanen

Ohjaaja: TkT Sami Suihkonen

III-nitridit, kuten alumiini-, gallium- ja indiumnitridi (AlN, GaN, InN) sekä niiden yhdisteet, valmistetaan tyypillisesti safiirialustakiteille. Tässä työssä perehdytään mahdollisuuksiin korvata safiiri piillä alustamateriaalina. Piin etuina safiiriin nähden on sen lämmön- ja sähkönjohtavuus. III-nitridien valmistaminen piikiekoille vähentäisi III-nitridipohjaisten komponenttien valmistuskustannuksia sekä mahdollistaisi perinteisen piiteknologian integroimisen III-nitridipohjaisiin komponentteihin.

Piin päälle valmistettavien III-nitridikerrosten valmistus aloitetaan tyypillisesti hilavakioiden eroja kompensoivan AlN-kerroksen valmistamisella. Työssä tutkittiin piin päälle plasma-avusteisella atomikerrosvalmistusmenetelmällä (PEALD, plasma-enhanced atomic layer deposition) valmistetun AlN-kalvon soveltuvuutta GaN:n valmistusalustana. AlN-kalvoja valmistettiin eri kidesuunnan omaaville piikiekoille ja tutkittiin lämpökäsittelyn vaikutusta niiden ominaisuuksiin. Kalvoja lämpökäsiteltiin eri lämpötiloissa sekä pikauunilla (RTP, rapid thermal processor) että perineisellä putkiuunilla (CTF, conventional tube furnace). Tutkimuksen päätteeksi AlN-kalvon päälle valmistettiin GaN-kalvo metallo-orgaanisella kaasufaasiepitaksialla (MOVPE, metallo-organic vapor phase epitaxy) ja tutkittiin valmistetun GaN-kalvon ominaisuuksia.

Valmistetut AlN-kalvot olivat noin 200 nm paksuja ja niiden todettiin olevan amorfisia röntgendiffraktiomittausten (XRD, X-ray diffraction) perusteella. Valmistetuissa kalvoissa ei havaittu reikiä eikä säröjä. Lämpökäsittelyn jälkeen kalvoissa havaittiin säröjä. Kalvot säilyttivät amorfisen luonteensa lämpökäsittelyssä. MOVPE:lla valmistetut GaN-kalvot olivat erittäin karheita sekä monikiteisiä.

Avainsanat: Lämpökäsittely, PEALD, alumiininitridi, pii

Author: Lauri Riuttanen

Title: Thermal Annealing of AlN Thin Films Fabricated by Plasma-Enhanced Atomic Layer Deposition for GaN Epitaxy

Date: 1.11.2010   Language: English   Number of pages:7+55

Faculty of Electronics, Communications and Automation

Department of Micro- and Nanosciences

Professorship: Optoelectronics   Code: S-104

Supervisor: Prof. Markku Sopanen

Instructor: D.Sc. (Tech.) Sami Suihkonen

III-nitrides, *e.g.*, aluminum, gallium and indium nitride (AlN, GaN, InN) and their alloys are typically grown on sapphire substrates. Silicon is an interesting candidate for substrate material for III-nitrides since it is electrically and thermally conductive unlike sapphire. The use of silicon substrates would also decrease the manufacturing costs of III-nitride-based devices. Another potential advantage is the integration of conventional silicon technology with III-nitride technology.

An AlN film is typically deposited on silicon before growing of GaN to compensate the lattice mismatch between the substrate and the grown layer. The suitability of AlN grown on silicon by plasma-enhanced atomic layer deposition (PEALD) as a substrate for GaN epitaxy was experimented in this thesis. Thermal annealing was performed to improve the crystalline quality of the deposited AlN. The AlN films were grown on silicon substrates having different orientations. The films were annealed both in rapid thermal processor (RTP) and in a conventional tube furnace (CTF). The films were characterized before and after the heat treatment. Finally, GaN films were deposited on the PEALD AlN film with metallo-organic vapor phase epitaxy (MOVPE) and characterized.

The thicknesses of the AlN films were about 200 nm and they were crack- and pinhole-free after deposition. X-ray diffraction (XRD) measurements indicated that the films were amorphous. Thermal annealing was found to induce cracks into the AlN films. After the annealing the films remained amorphous. GaN films grown by MOVPE were extremely rough polycrystalline films.

Keywords: Thermal annealing, PEALD, aluminum nitride, silicon

Preface

This thesis was carried out in the Department of Micro and Nanosciences at Aalto University School of Science and Technology.

First I would like to thank Professor Markku Sopanen for giving me a chance to complete my thesis in the laboratory and my instructor Sami Suihkonen for good guidance and help in understanding this research. Additionally, I would like to express my gratitude to Markus Bosund for providing me material for this research, Olli Svensk for his expertise in MOVPE growth process, Sakari Sintonen for his knowledge on X-ray analysis and the rest of the staff members, who helped me in using the measurement and processing equipment and providing me all around knowledge and inspiring conversations.

Finally, I would thank my friends and family for supporting me on my thesis and through my education.

Otaniemi, 1.11.2010

Lauri J. Riuttanen

Contents

Symbols and Abbreviations

Symbols

a, c	Lattice constants
$\mathbf{a_i}$	i^{th} lattice vector
h,k,(i),l	Miller(-Bravais) indices

Abbreviations

AFM	Atomic force microscope
ALD	Atomic layer deposition
AlN	Aluminum nitride
CTE	Coefficient of thermal expansion
CTF	Conventional tube furnace
FCC	Face centered cubic
GaN	Gallium nitride
HF	Hydrofluoric acid
InN	Indium nitride
LED	Light emitting diode
MBE	Molecular beam epitaxy
MOCVD	Metallo-organic chemical vapor deposition
MOVPE	Metallo-organic vapor phase epitaxy
PEALD	Plasma-enhanced atomic layer deposition
PID	Proportional-integral-derivative
RF	Radio frequency
RTA	Rapid thermal annealing
RTP	Rapid thermal processor
SE	Spectroscopic ellipsometer
SEM	Scanning electron microscope
TE	Transverse electric
TEM	Transmission electron microscope
TMAl	Trimethylaluminum
TMGa	Trimethylgallium
TMIn	Trimethylindium
UV	Ultra violet
XRD	X-ray diffraction
XRR	X-ray reflectivity

1 Introduction

III-V semiconductor alloys are important materials for manufacturing optoelectronic devices. III-nitrides, *e.g.*, indium, aluminum and gallium nitride (InN, AlN, GaN) are semiconductors with direct band gap. III-nitride alloys are suitable for short wavelength devices, such as green, blue and ultra violet (UV) light emitting diodes (LED) and laser-diodes. GaN-based LEDs are already in commercial use in color displays and lighting [1, 2]. Single crystal GaN can also be used to fabricate high power, high frequency transistors.

Usually sapphire has been used as a substrate for GaN-based devices. Sapphire is thermally and electrically insulating material which causes costs through complex after growth processing. One promising substrate candidate is silicon. Silicon wafers are readily available in large sizes and they are cost efficient due to long history of silicon technology. Additionally silicon is thermally and electrically conductive unlike sapphire. Another interesting point in using silicon as a substrate for GaN-based devices is the possibility to integrate conventional silicon technology with GaN technology.

The growth of GaN on silicon has been studied by different research groups. There are problems due to different crystal structure of silicon and GaN. Also lattice mismatches and different coefficients of thermal expansion (CTE) induce difficulties in GaN growth. Despite the problems there has been successes in growing GaN on silicon, *e.g.*, F. Reiher *et al.* have realized an InGaN/GaN LED structure grown on (1 1 0)-oriented silicon substrate. Light emission with a peak at 490 nm was obtained by electrical excitation. [3]

Growth of GaN on silicon is not usually carried out directly on silicon. An AlN seed layer is often used. [3] The reason behind this approach is to give a better starting point for epitaxial growth of GaN. The crystal structure of single crystal silicon is diamond, hence wurtzite GaN or AlN cannot be grown epitaxially on silicon. However, polycrystalline AlN film can be deposited and it acts as a seed layer for epitaxial growth of GaN. LEDs rely on properties of electronic band structure of single crystal semiconductors. Dislocations act as non-radiative recombination centers. It is imperative to grow single crystal semiconductor with low dislocation density for manufacturing good quality LEDs.

The crystal quality of the grown epilayer depends on the crystal quality of the substrate. In growing GaN on silicon with an AlN seed layer, the crystal quality of the seed layer has a great impact on the quality of the grown GaN film. Rapid thermal annealing (RTA) can be used for improving the crystal structure of crystalline material. In the case of III-nitrides it may balance the fluctuations of nitrogen concentration and reduce crystal defects generated during the growth of the layer [4]. Thermal annealing gives energy to atoms for rearranging and the grains in polycrystalline material start to grow and smaller grains can merge into larger ones.

The goal of this thesis was to study the possibility to use silicon with plasma-enhanced atomic layer deposition (PEALD) grown AlN seed layer as a substrate for

GaN. AlN films were grown with PEALD on silicon wafers with different crystal orientations. The effect of RTA treatment on crystallinity and topography of AlN films was also studied. A conventional tube furnace (CTF) was used as a reference annealing method. The suitability of PEALD grown AlN layer on silicon was tested by growing GaN layers with metallo-organic vapor phase epitaxy (MOVPE) on top of the AlN layer.

Chapter two discusses the basics of crystal structures and the differences between silicon and AlN lattices. The theory of crystal structures is needed to understand the growth dynamics of thin films. Also the effect of thermal annealing is discussed. It is crucial to understand how temperature changes affect different materials. Previous studies concerning growth of AlN on silicon by atomic layer deposition (ALD) and thermal annealing of AlN films are discussed in chapter three. The information obtained from literature was used as a base for this research. Equipment and methods used to fabricate and characterize the samples are presented in chapters four and five, respectively. The chapters consist of an overview of basic principles and limitations of the used equipment. The details and the process parameters of the experimental work are described in chapter six. Results are presented and discussed in chapter seven. The conclusions of this research are presented in chapter eight.

2 Theory

The following chapter gives a short introduction to the physics behind this work. While AlN layer is grown on silicon to obtain substrate for epitaxial GaN, it is crucial to understand what kind of properties crystalline materials have and how different crystal structures differ from each other. Also it is imperative to understand how solids behave in high temperatures and how they act under temperature changes.

2.1 Crystal Structures

If atomic structure of solid material is periodic in all directions, it is considered to be crystalline material, which is built from small building blocks called unit cells. A unit cell is the smallest periodic structure in a crystal lattice. The unit cell is defined by lattice vectors $\mathbf{a_1}$, $\mathbf{a_2}$, $\mathbf{a_3}$. Any point of the lattice can be obtained from an other lattice point by using these lattice vectors. This kind of lattice is called a Bravais lattice. The vector $\mathbf{a_1}$ is usually defined by the shortest period in the lattice. In the case of cubic cells $\mathbf{a_2}$ is perpendicular to $\mathbf{a_1}$, and $\mathbf{a_3}$ is perpendicular to the plane spanned by $\mathbf{a_1}$ and $\mathbf{a_2}$. For the lattice constant of cubic cell applies $|\mathbf{a_1}| = |\mathbf{a_2}| = |\mathbf{a_3}| = a$, in which a is the lattice constant of the crystalline material. [5]

Miller's indices are used to denote place, crystal directions and planes of a crystal lattice. A Miller index consists of three integers h, k and l. These integers are used as coefficients for the lattice vectors. Negative coefficients are noted with a bar, *e.g.*, $-\mathrm{h} = \bar{\mathrm{h}}$. A crystal direction in the lattice is noted in form [h k l]. The form <h k l> can be used, if the directions are symmetric. Crystal directions are considered symmetrical, if <h k l> = <$\bar{\mathrm{h}}$ $\bar{\mathrm{k}}$ $\bar{\mathrm{l}}$> applies. [5]

The notation for a crystal plane is (h k l) and, if the crystal planes are symmetric, notation {h k l} can be used. A crystal plane is defined with points in which the plane intersects the axes of the crystal lattice. The reciprocal is taken from those coordinates and they are reduced to the smallest integers. [5] *E.g.*, if the crystal plane intersects x-, y- and z-axes in coordinates (1;0;0), (0;2;0) and (0;0;3), the plane is noted (6 3 2). The crystal directions and the crystal plane (6 3 2) are presented in figure 1.

Material is considered to be a single crystal, if it consists of continuous lattice formed by unit cells (*e.g.*, a typical silicon wafer). Material is considered to be polycrystalline, if it consists of mixed oriented grains of crystals (*e.g.*, most metals). Material is amorphous, if long-range periodicity does not exist. Single crystalline material always has some defects. Defects can be categorized as point defects, line defects, plane defects and volume defects. Examples of point defects are vacancies, interstitial atoms and substitutional atoms. Line defects are also known as dislocations and can be considered as defect sites that can be connected by a line. When considering ideal polycrystalline material, the grains are perfect crystals. The grain boundaries are an example of planar defects. They can also be seen as an array of dislocations. Examples of volume defects are voids and regions of amorphous material inside the
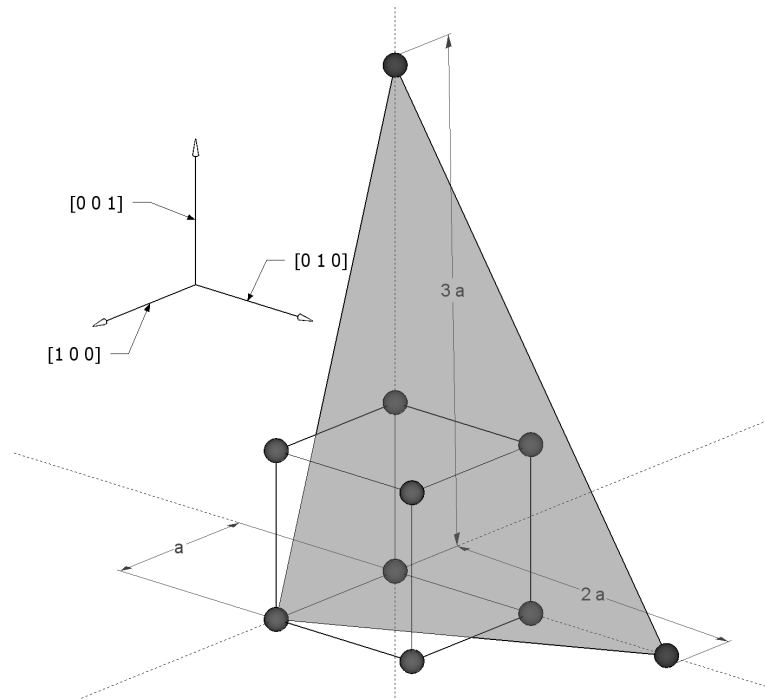
Figure 1: Unit cell of the simple cubic lattice and the crystal plane (6 3 2). The lattice constant is noted with a.

grown crystal. [5]

Diamond Structure

Silicon crystallizes in diamond structure. A diamond cell can be thought as two face centered cubic (FCC) cells, which are displaced along the body diagonal direction. The FCC lattice is a cubic lattice in which the center of each face of the cube has an atom in addition to the atoms in the corners of the cube. As diamond cell is a cubic cell, relation $|\mathbf{a_1}| = |\mathbf{a_2}| = |\mathbf{a_3}| = a$ applies for the length of the lattice vectors. The lattice constant of silicon is 5.43 Å. Also the lattice vectors are perpendicular to each other. Crystal directions and planes of silicon are symmetric so notations $<>$ and $\{\}$ can be used. The diamond lattice is shown in figure 2 from different crystal directions.
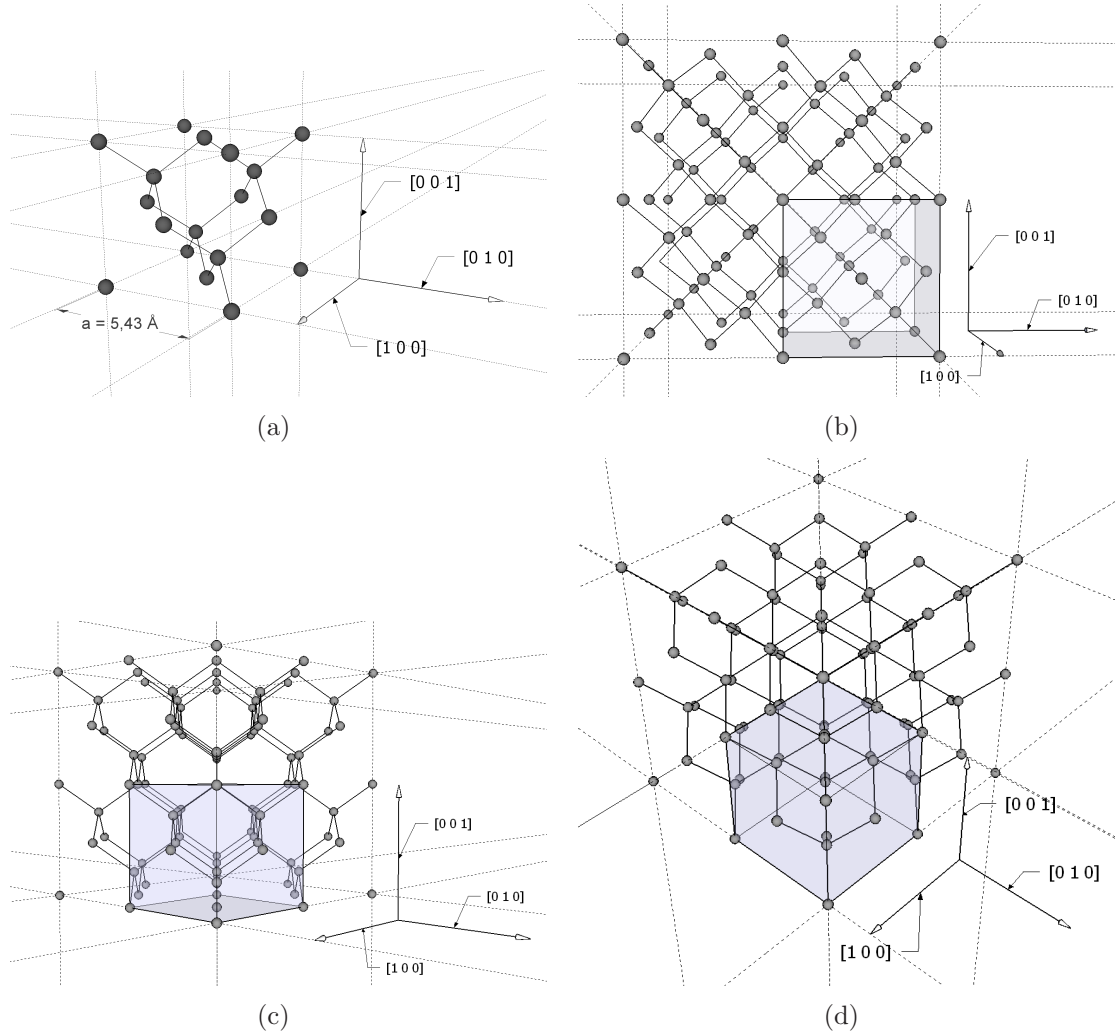
Figure 2: Silicon crystallizes into a diamond structure with a lattice constant of 5.43 Å. (a) A unit cell of the diamond structure. The diamond lattice shown from directions (b) [1 0 0], (c) [1 1 0] and (d) [1 1 1].

Wurtzite Structure

III-nitrides can crystallize in wurtzite, zinc blende or halide structures. Wurtzite structure is the only thermodynamically stable structure in normal conditions for InN, GaN and AlN. [6] Therefore, only wurtzite structure, which is a hexagonal structure, is presented in this thesis. The directions and planes of hexagonal lattice can be noted as in a cubic lattice, but often they are noted with four integers instead of three. The four integer notation is called the Miller-Bravais index. By using the Miller-Bravais notation it is seen right away that the lattice structure is hexagonal. The Miller-Bravais index for hexagonal structure is in the form [h k i l], in which i = -h -k. The same applies for the crystal planes. In an ideal wurtzite lattice $|\mathbf{a_1}| = |\mathbf{a_2}| = a$ and $|\mathbf{a_3}| = c$, where a and c are the lattice constants of the wurtzite lattice. The angle between $\mathbf{a_1}$ and $\mathbf{a_2}$ is 120° and $\mathbf{a_3}$ is perpendicular to the plane

spanned by $\mathbf{a_1}$ and $\mathbf{a_2}$.

III-nitrides can crystallize as M-polar or N-polar. M corresponds to metal and N to nitrogen atoms. The polarity of the crystal structure is determined by the atoms on the basal plane. If the basal plane of AlN consists of aluminum atoms, the crystal is Al-polar and, if it consists of nitrogen atoms, it is N-polar. The wurtzite unit cell and the lattice typical for AlN are shown in figure 3.
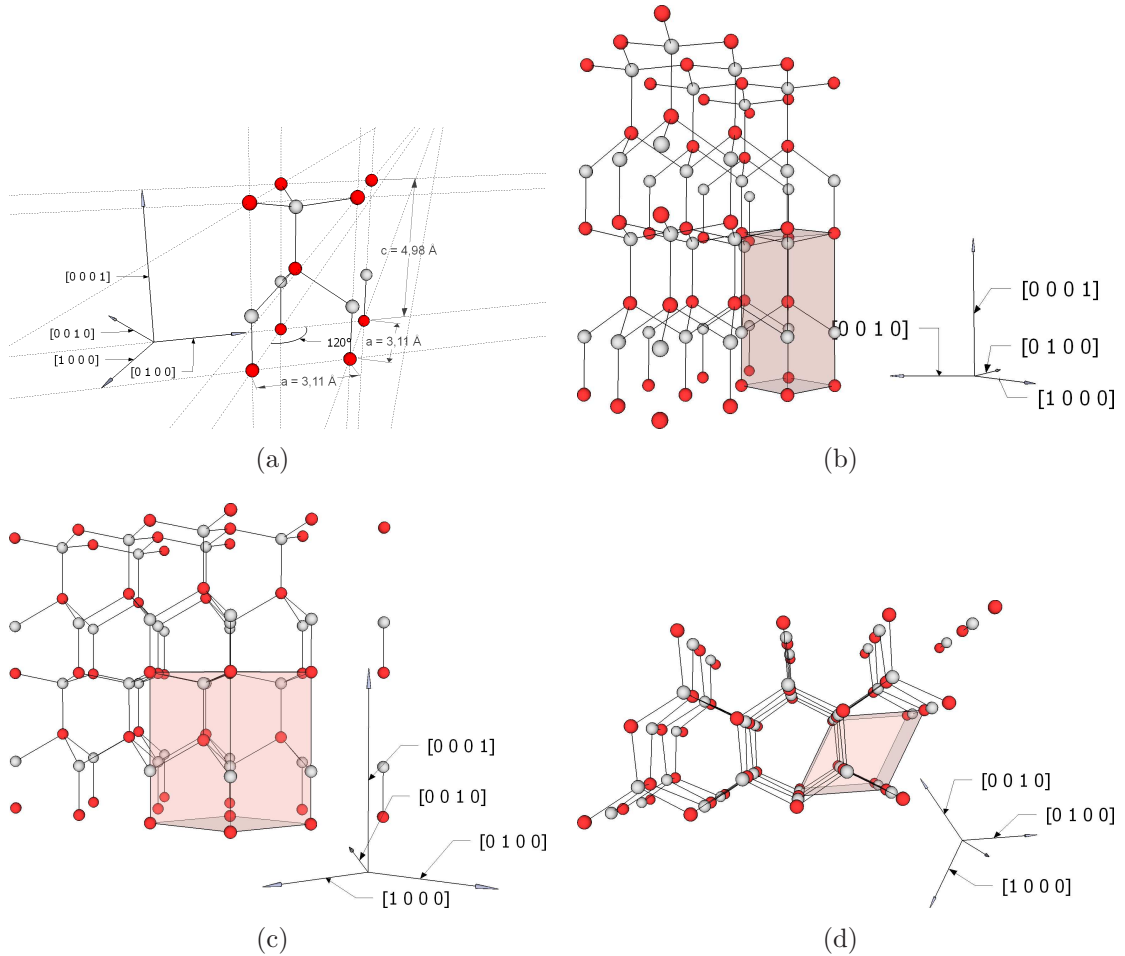

Figure 3: Al-polar wurtzite aluminum nitride. Aluminum atoms are drawn with red and nitrogen atoms with grey. (a) A unit cell and the lattice shown from directions (b) [1 $\bar{1}$ 0 0], (c) [1 1 $\bar{2}$ 0] and (d) [0 0 0 1].

Aluminum Nitride Lattice on Silicon Substrate

An AlN seed layer can be used to grow c-axis, *i.e.*, (0 0 0 1)-oriented GaN on silicon [3]. Wurtzite AlN is difficult to grow epitaxially on silicon due to their different crystal structures. The deposited AlN will end up to be more or less polycrystalline or amorphous. The interfacial structure of the deposited AlN and the silicon substrate depends on the crystal orientation of the silicon substrate. This is due to the different atomic arrangement of silicon atoms on the crystal planes.

AlN films have been grown on silicon wafers with the most common orientations, *i.e.*, (1 0 0), (1 1 0) and (1 1 1) [7, 8, 9]. AlN growth on (1 0 0)-oriented silicon substrate is considered challenging due to the different type of surface reconstructions. The quality of devices grown on (1 0 0)-oriented silicon substrate is inferior compared to devices grown on (1 1 1)-oriented silicon substrate. The three-fold atomic arrangement of (1 1 1)-plane of silicon is compatible with basal planes of wurtzite type crystals. The lattice mismatch of c-plane of AlN and (1 1 1)-plane of silicon is 19% which leads to high density of dislocations in the AlN seed layer. [3] The (1 1 0)-oriented silicon substrate is interesting due to a small lattice mismatch of only 0.8% parallel to c-plane of AlN and (1 1 0)-plane of silicon [8]. For comparison, lattice mismatch of sapphire and GaN is 13% [1]. Transmission electron microscope (TEM) images and schematic illustrations of atomic arrangement in cross section of the interaface between AlN and silicon with orientation of (1 1 0) and (1 1 1) are shown in figure 4.
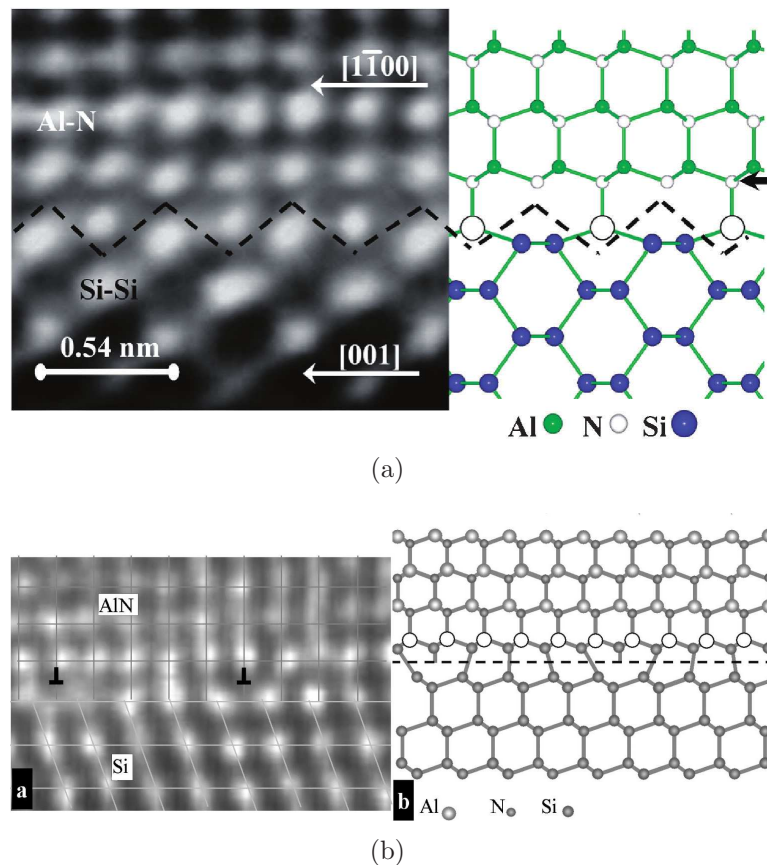

(a)

(b)

Figure 4: TEM images and schematic models of atomic arrangement in the interface between AlN and silicon with orientation of (a) (1 1 0) and (b) (1 1 1). Open circles in the images can be N, Al or Si atoms. Misfit dislocations are marked with tickmarks. [7, 8]

2.2 Effects of Thermal Annealing

In solids atoms interact with each other through repulsive and attractive forces. In a crystalline material each atom is bound to an equilibrium position by those interatomic forces. Those forces can be seen as springs, which allow the atoms to vibrate near their equilibrium position. As the temperature rises the atoms gain more kinetic energy and their vibration amplitude grows. [10] The excess kinetic energy of the atoms allows them to rearrange in the crystal lattice. It also increases diffusion of atoms in the material. This may lower fluctuations of concentrations in the annealed material. Annealing improves the crystal quality of crystalline material by reducing defects in the crystal lattice and allowing grain growth of polycrystalline material.

Most materials expand when heated due to thermal expansion. As stated before, it can be understood that atoms are connected to each other with springs. As thermal energy is brought to the material, the vibration amplitude starts to increase. With most solids the spring forces act in a way that they expand easier than compress. Hence the average distance between the atoms becomes larger and material expands in every dimension. The coefficient between temperature change and expansion is called coefficient of thermal expansion (CTE). [10]

CTE is a material specific property and it can also have negative values. It is also temperature dependent (*e.g.*, the density of water is highest at 4 °C). Thermal expansion occurs in all materials independent of the phase, *i.e.*, in gases, liquids and solids. CTE mismatch has to be taken into account in growth and thermal annealing of thin films. If the deposited film has a larger CTE than the substrate, the deposited film experiences compressive stress, when temperature is increased and vice versa. The stress introduced during annealing, compressive or tensile, is called thermal stress. Thin films may form cracks or other defects to relieve excessive stress.

The effect of thermal annealing on stress can be easily derived by using a one dimensional example. Assuming that a rod of arbitrary material has a length of L_0 and it's thermal expansion coefficient is α the change in length by thermal expansion ΔL of the rod can be stated

$$\Delta L = \alpha L_0 \Delta T, \tag{1}$$

where ΔT is change in temperature. We can now state the fractional change in length introduced by the thermal expansion

$$\left(\frac{\Delta L}{L_0}\right)_{thermal} = \alpha \Delta T. \tag{2}$$

If the rod is clamped from both ends, the stress must increase in the opposite direction to compensate the change in length introduced by the thermal expansion. The fractional change in length by stress can be calculated with Hooke's law

$$\sigma = Y\epsilon, \tag{3}$$

in which σ is the stress perpendicular to the rod, Y is Young's modulus of the rod and ϵ is the fractional change in length by stress. As stated before, the change in length by stress is equal and opposite to the change in length by thermal expansion

$$\epsilon = \left(\frac{\Delta L}{L_0}\right)_{stress} = -\left(\frac{\Delta L}{L_0}\right)_{thermal} = -\alpha\Delta T. \tag{4}$$

This results in

$$\sigma = -Y\alpha\Delta T. \tag{5}$$

As seen in equation 5, the total stress induced by the annealing is dependent of the total temperature change and the material parameters. The temperature dependency of the coefficient of thermal expansion can be added to the equation and equation 5 can be written in integral form

$$\sigma = -\int_{T_0}^{T_1} Y\alpha(T)\, dT, \tag{6}$$

where T_0 is temperature in the zero stress state and T_1 is the target temperature. The three dimensional equation can be derived in a similar way. As seen in equation 6, the thermal stress introduced is independent of the ramp rate. However, the high ramp rate may cause large temperature gradients which leads to localized thermal stress. If we consider a thin film deposited on a substrate with lower CTE than the CTE of the thin film and we assume that the thin film is relaxed during the steady state of the annealing, the thin film will be in tensile stress after the annealing process.

3   Previous Studies

The literature on ALD grown AlN films and thermal annealing of AlN films was reviewed and the information was used as a base for the research.

3.1   Aluminum Nitride Films Deposited on Silicon Substrates by ALD

There has been several studies in which AlN films on (1 0 0)-oriented silicon wafers have been realized by ALD and the effect of different deposition parameters has been studied. AlN films can be deposited with both thermal ALD and PEALD. Usable precursors for aluminum in ALD processes are trimethylaluminum (TMAl) and aluminum chloride. Ammonia is typically used as the precursor for nitrogen in a thermal ALD process. In the PEALD process ammonia is dissociated to nitrogen and hydrogen radicals with a plasma discharge. The plasma generated radicals act as a precursor. Growth temperatures used in studies varied from 200 to 470 °C and the plasma power varied from 50 to 300 W. Typical radio frequency (RF) to generate plasma was 13.56 MHz. [9, 11] It has been shown that the deposition rate of AlN is considerably higher with PEALD compared to thermal ALD. Higher plasma power resulted in a higher deposition rate and increased the wafer non-uniformity. It was suggested that the non-uniformity was due to poorer ion concentration distribution at higher plasma powers. With X-ray diffraction (XRD) analysis it has been shown that AlN films grown by PEALD are polycrystalline at a sufficient growth temperature, *i.e.*, over 370 °C. Higher growth temperatures resulted in higher deposition rate and better crystal quality. The root mean square roughness of deposited AlN films increased with increasing films thicknesses. [11] Studies concerning ALD deposition of AlN films on silicon with orientation (1 1 0) or (1 1 1) were not found in the literature.

3.2   Thermal Annealing of Aluminum Nitride

The effect of thermal annealing on crystal quality, morphology and electrical properties of AlN films on silicon wafers grown by RF sputtering has been studied [12, 13]. Annealing of AlN films grown on sapphire substrate with MBE has also been studied [4]. In these studies the samples were annealed in nitrogen ambient at temperatures ranging from 400 to 1300 °C. The temperature ramp up rate varied from 50 to 60 $\frac{°C}{s}$ and ramp down rate from 40 to 50 $\frac{°C}{s}$. Studied annealing time ranged from 10 to 90 s. In XRD measurements crystal quality was shown to improve when the annealing temperature was over 600 °C. Relying on XRD measurements it has been proposed that AlN film starts to degrade when it is annealed at over 1200 °C. The polycrystalline films, which were highly c-orientated became more c-orientated. It was proposed that this was due to merging of amorphous material in grain boundaries into larger c-oriented crystals. In XRD measurements the diffraction peaks had

shifted indicating that the thermal annealing had introduced tensile stress into the AlN film. Thermal annealing with temperature ramp up rate $60 \frac{°C}{s}$ at temperatures of over 1000 °C introduced also microcracks into the surface of AlN films. [4, 12, 13]

4 Sample Fabrication Equipment

AlN films were deposited with plasma-enhanced atomic layer deposition (PEALD) on silicon wafers. After depositing the AlN film the samples were characterized and annealed in a RTP. In contrast to the fast process of RTP a conventional tube furnace (CTF) was also used. After examining the annealed films, GaN was grown on them with MOVPE. Depositing of AlN film and rapid thermal annealing of the samples were done in the cleanroom of Micronova building. Annealing in the tube furnace and the MOVPE process was performed in smaller cleanrooms also located in the Micronova building.

4.1 Atomic Layer Deposition

ALD is a gas phase deposition process. With ALD it is possible to deposit thin films with a precision of one atomic layer. ALD process was developed in the 1970's by Tuomo Suntola for manufacturing electroluminescence flat panel displays. Advantages of ALD are good selection of materials for depositing, low process temperatures, precision on film thicknesses, good film uniformity and conformal deposition of films. [14]

The basic principle of ALD process is to bring source gases one by one in pulses to the reaction chamber and purge it in between with an inert gas. Typical cycle consists of four steps. First the chamber is filled with the first source gas and the gas flow is kept on for sometime to let molecules adsorb to the surface of the substrate. Then the chamber is purged with an inert gas. After purging the chamber is filled with the second source gas. Finally the chamber is purged again. The number of cycles determines the deposited film thickness. Growth rate can vary in the beginning of the growth process due to reaction capabilities of the substrate. When the number of cycles increases, the growth rate becomes linear. [14]

To expand the variety of materials, which can be deposited with ALD, more aggressive reactants are needed. For this purpose radicals can be generated by dissociation of gases with a plasma source. Such ALD process is called plasma-enhanced atomic layer deposition (PEALD). In a PEALD process the target substrate is located very near or inside the plasma discharge. [15]

For this work AlN films were fabricated by PEALD using TMAl as the precursor for aluminum. Ammonia was used as the precursor for nitrogen. Ammonia is dissociated into nitrogen and hydrogen radicals with a plasma discharge. Both radicals participate in the PEALD process, which is illustrated in figure 5. The silicon substrate is dipped in hydrofluoric (HF) acid prior to the growth. The HF dip removes native oxide from the silicon substrate and makes the surface hydrogen-terminated. First TMAl is brought into the reaction chamber with nitrogen as carrier gas. The TMAl molecules substitute hydrogen atoms of the hydrogen-terminated silicon substrate. After purging the chamber plasma is switched on and ammonia is cracked into hydrogen and nitrogen radicals. Radicals are brought to the reaction chamber

and nitrogen radicals substitute the methyl groups of TMAl molecules and a AlN monolayer is formed. The methyl molecules react with hydrogen radicals forming methane as a by-product. Beneq TFS-500 ALD system was used for the PEALD process.
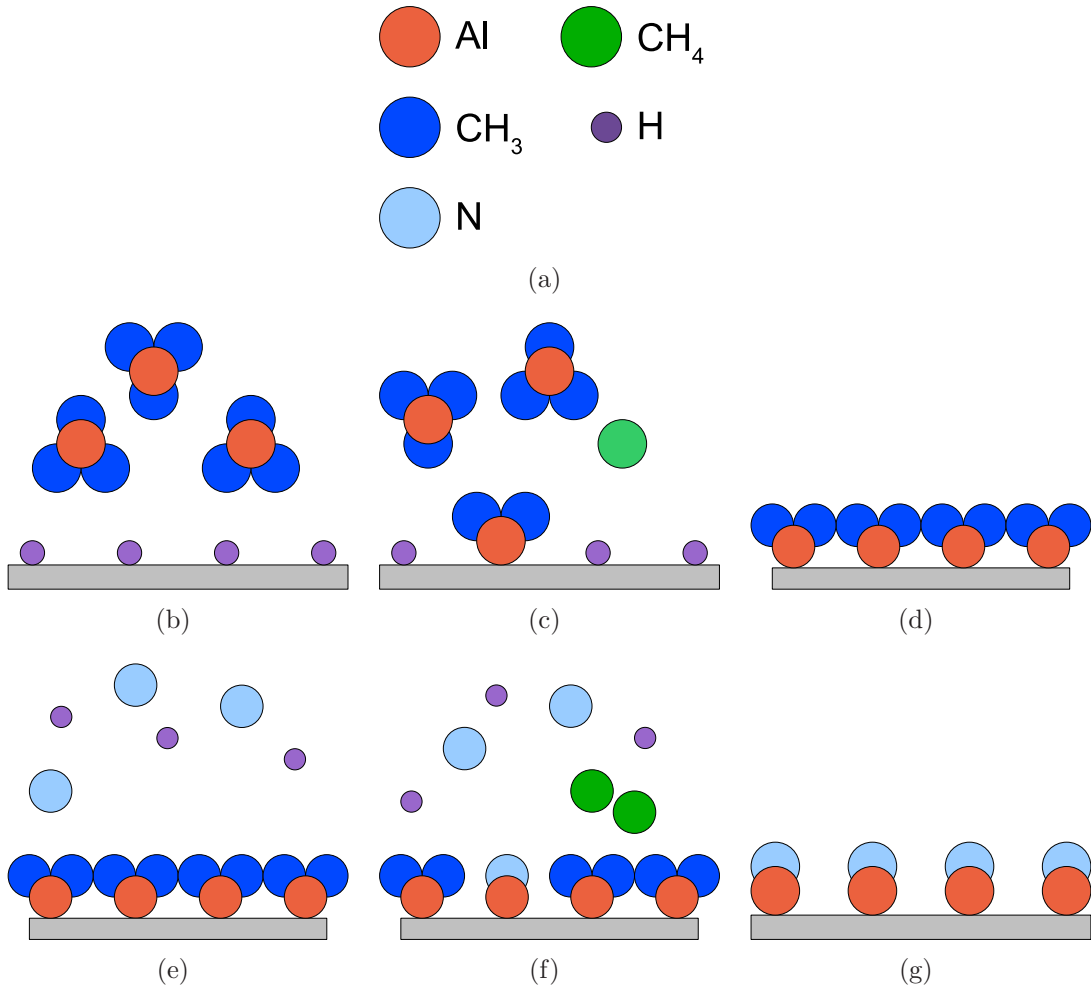
Figure 5: Schematic illustration of a PEALD cycle. (a) Legend of atoms and molecules participating in the process. (b) Substrate is a hydrogen terminated silicon wafer and TMAl is brought into the chamber. (c) TMAl molecules substitute hydrogen atoms from the surface giving away one methyl group to the hydrogen atom substituted. Hydrogen and methyl-group form methane as a by-product. (d) The surface saturates from dimethylaluminum and the chamber is purged. (e) Plasma generated hydrogen and nitrogen radicals are brought to the sample. (f) Nitrogen substitutes two methyl groups for each aluminum. Substituted methyl groups and hydrogen radicals form methane as a by-product. (g) The aluminum atoms saturate from nitrogen and the chamber is purged. The number of cycles determines the layer thickness.

4.2   Annealing Furnaces

Thermal annealing was performed with RTP and a conventional tube furnace (CTF). In a tube furnace the sample is placed in a quartz tube, which is heated. The used tube furnace has three heating zones to obtain homogeneous temperature distribution. During heating the sample was subjected to a nitrogen gas flow.

In RTP samples are subjected to high temperatures for a reasonably short period of time. The reaction chamber can be filled with gas, pumped down to vacuum or kept filled with room air during the annealing. The process gases vary according to the process. Typical process gases are inert, *e.g.*, argon or nitrogen. Also oxygen can be used, if the process is used for oxidation. Jipelec JetFirst 200C RTP was used for RTA processing.

Heating in Jipelec JetFirst 200C RTP is done with 18 infra red lamps. For measuring the process temperatures a pyrometer was used. Annealed sample was located on a susceptor and the pyrometer measured temperature optically from the bottom of the susceptor.

PID Controller

Temperature controlling in the used RTP is carried out with a proportional-integral-derivative (PID) controller. During this work the PID tables of the RTP were configured for the first time. PID controllers are widely used for controlling different systems. They cover majority of controlling problems. In a typical PID setup a feedback loop is used to obtain the difference between the setpoint and the measured output. This so called error signal is fed through proportional, integrating and derivating blocks. These three functional blocks are parallel and their output is summed together. The proportional block affects the input with a proportion to the measured error, the integrating block with a sum of recent errors and the derivating block with a rate in which the error is changing. The sum is used to drive the process, *e.g.*, the heating of the chamber of the RTP. The gain of each block of the PID can be tuned individually with parameters P, I or D, respectively. Schematic illustration of PID-controlled process is shown in figure 6.

Using only a proportional (P) controller the output at steady state never reaches the setpoint. This steady state error is called droop. Adding an integrating term (I) to the controller eliminates the droop, but it induces overshoot due to error accumulated from the past. The overshoot can be reduced by adding a derivate term (D) to the controller, but it slows the rate of change of the output. As stated before, a PID controller uses all three terms: P,I and D. Poor choices of the gains of the functional blocks of the PID controller causes the system to be unstable. In the used RTP the PID tables can be tuned for several temperature intervals individually.
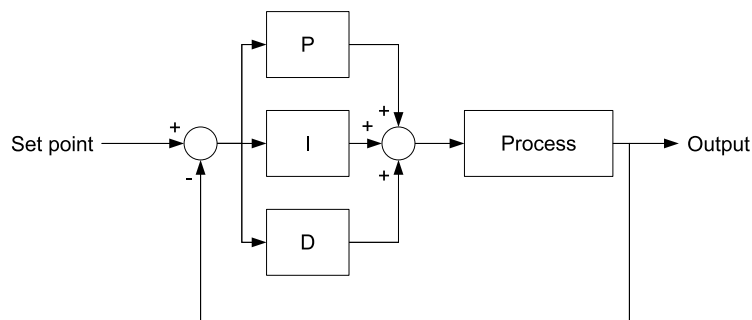
Figure 6: Block diagram of a PID-controller. Error, *i.e.*, difference between a given setpoint and measured output is fed through proportion, integrating and derivating blocks. Outputs of those blocks are summed together. This signal is used to drive the process.

4.3   Metallo-Organic Vapor Phase Epitaxy

Metallo-organic vapor phase epitaxy (MOVPE), also known as metallo-organic chemical vapor deposition (MOCVD), is a gas phase deposition method for growing semiconductor materials. In epitaxial growth the deposited film copies the crystal structure and orientation of the substrate material. The name MOVPE stems from the precursor gases used in the process. In the case of III-V semiconductors the precursors for group III materials are metallo-organics, *i.e.*, materials, which consist of molecules composed of a metal atom and hydrocarbons. [16] In a MOVPE reactor precursor gases are conducted in a continuous carrier gas flow to the heated substrate. The precursor gases decompose at high temperature near the substrate and the atoms adsorb to the surface of the substrate. [17]

Typical precursors for aluminum, gallium and indium are liquid trimethylaluminum (TMAl), trimethylgallium (TMGa) and trimethylindium (TMIn), respectively. The metallo-organics are kept in temperature controlled steel containers called bubblers. The carrier gas is flown through the bubblers and it saturates from the liquid metallo-organic. Gaseous ammonia is used as a precursor for nitrogen. Typical dopants for GaN are magnesium for p-type GaN and silicon for n-type GaN. The group III and group V precursors are brought into the reaction chamber in different gas manifolds and mixed in the reaction chamber to minimize prereactions between precursors. A schematic illustration of the gas lines of a MOVPE reactor is shown in figure 7. [18]

Growth of GaN is typically heteroepitaxy due to the lack of reasonably priced good quality GaN substrates. Typical substrates used are sapphire and silicon carbide (SiC). Due to the high cost of good quality SiC sapphire is preferred. [16] Silicon is an interesting substrate candidate, since silicon is more cost efficient than sapphire and it is compatible with conventional silicon technology. In addition, silicon conducts heat well.

Two-step process is typically used in MOVPE growth of III-nitrides on foreign substrates. In a two-step process a thin low temperature nucleation layer of GaN or
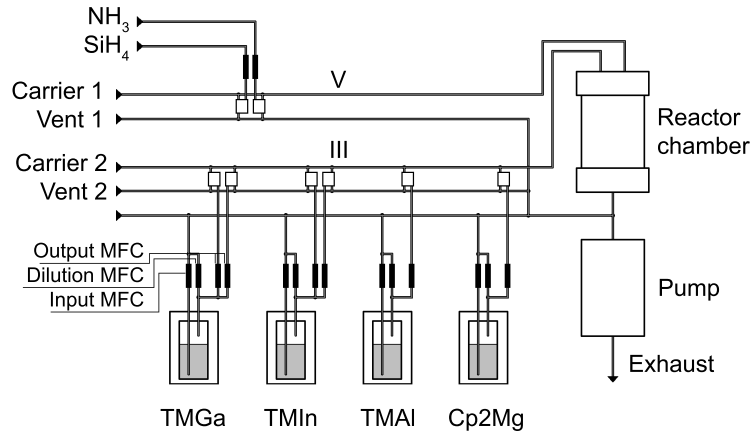
Figure 7: A schematic illustration of the gas lines of a MOVPE reactor. Carrier gas is flown through bubblers containing liquid metallo-organic precursors. The gas flows are controlled with mass flow controllers, denoted as MFCs in the figure. Group V precursor and n-type dopant gas is mixed with carrier gas and fed into the reaction chamber through a different manifold than the metallo-organic precursors and p-type dopants for minimizing prereactions. [18]

AlN is first grown on the substrate. Typical growth temperature of the nucleation layer is around 500 °C. The second step is the actual growth, which is performed at high temperature, around 1000 °C. Due to the mismatch of the lattice constants between the substrate and the grown layer the nucleation layer forms islands, when the temperature of the reactor increases. During the actual high temperature growth the islands coalesce and the epilayer growth begins. The growth is observed with *in-situ* reflectometer.

The two-step growth process can be divided in 7 stages according to the readout of the reflectometer. Example of reflectometer readout as a function of growth time and schematic illustration of surface morphology of different stages is presented in figure 8. The growth process typically begins with a substrate preparation, *i.e.*, baking and nitridation. After the substrate has been prepared, the growth of nucleation layer begins. In the first stage the low temperature nucleation layer starts to grow and the reflectance increases or decreases depending on the properties of the substrate and grown layer, *e.g.*, it increases when GaN is grown on sapphire. The morphology of the grown nucleation layer is smooth. When the nucleation layer is thick enough, *i.e.*, more than 50 nm or less than 100 nm, the precursor gases are put to by-bass flow and the temperature is ramped up to the actual growth temperature. The material in the nucleation layer starts to recrystallize and it partially decomposes. The nucleation layer starts to form islands and the reflectance rapidly decreases due to surface roughening. As the material decomposes it starts to expose the surface of the substrate and the readout from the reflectometer starts to increase again. When the density and the size of the islands are desired, the precursor gases are flown again to the reaction chamber and the high temperature growth begins. The islands start 3-dimensional growth, *i.e.*, lateral and vertical growth. This de-

creases the readout from the reflectometer. When the islands start to coalesce, the reflectance increases due to smoothening of the surface morphology. The readout from the reflectometer starts to oscillate after the islands are fully coalesced. The oscillations are due to interference between beams reflected from different interfaces in the sample. [18]
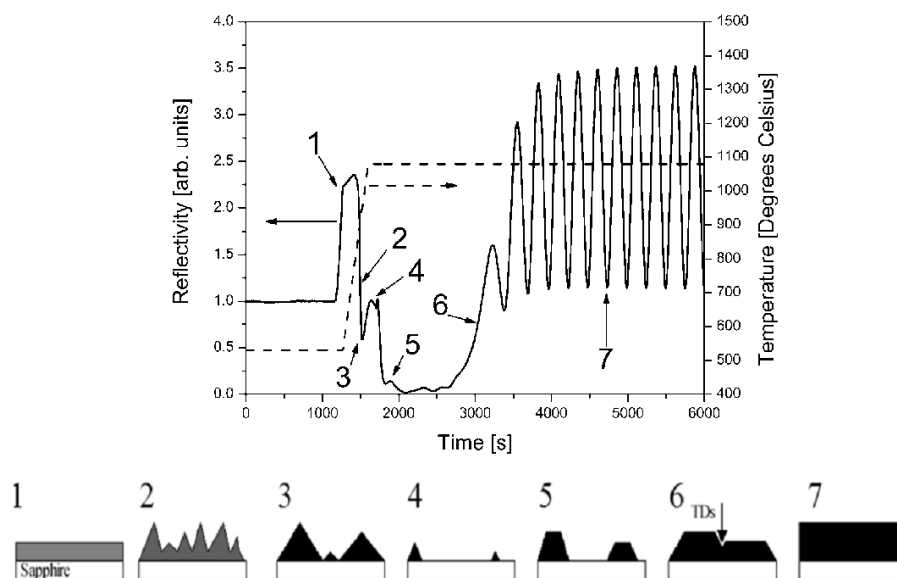

Figure 8: An example of *in-situ* reflectometer readout during MOVPE growth of GaN and a schematic illustration of surface morphology. (1) A low temperature nucleation layer is formed and the reflectance increases. Temperature is increased to the growth temperature and the nucleation layer starts to recrystallize and material starts to decompose. (2) The increase in surface roughness decreases the readout. (3-4) The nucleation layer starts to form islands and exposes the surface of the substrate. (4-5) The high temperature growth starts and the islands begin to grow. (6) Islands coalesce and the reflection increases. (7) When islands have been fully coalesced, the surface of the grown film is flat and reflectance oscillates due to interference. [19]

5 Measurement Equipment

The used measurement equipment is presented in this chapter. All the measurements were performed in the Micronova building.

5.1 X-ray Reflection and X-ray Diffraction

In X-ray diffraction (XRD) and X-ray reflectivity (XRR) measurements the sample is subjected to X-ray radiation. X-ray radiation used in these measurements consists of X-ray photons from the $K\alpha_1$-line of copper. The wavelength of these X-ray photons is 1.540560 Å. [20]

X-rays interact with materials in many ways depending on the properties of the material and the radiation. When a X-ray photon hits material, it can reflect from, absorb into, penetrate or scatter from the material. [20] A schematic set up of these X-ray measurements is shown in figure 9. The sample can be rotated along the angles Ψ, Φ and ω marked in the figure. In a symmetrical scan the detector and the sample are moved in such a way that the relation $\theta = \omega$ is preserved.
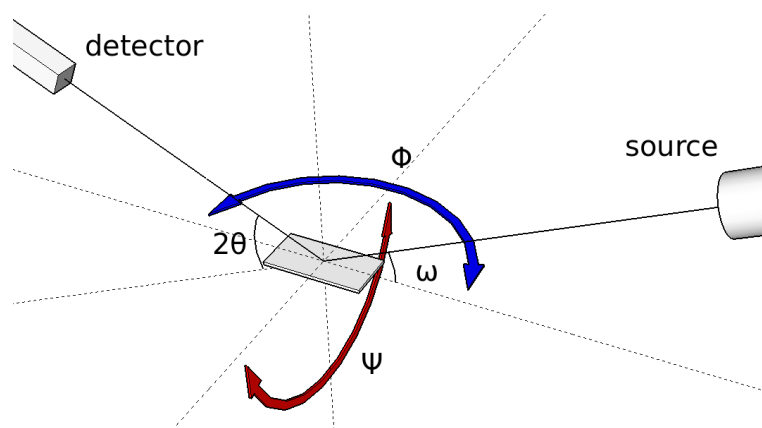

Figure 9: A schematic image of X-ray measurements. The sample is illuminated with X-ray photons with an incident angle of ω, which is defined in respect to the surface of the sample. The X-ray beam scatters or reflects in an angle of 2θ respective to the incident beam. The beam is measured with a X-ray detector. The sample can be rotated in three directions Ψ, Φ and ω.

XRD measurements can be used to get data from the crystal properties of crystalline material due to scattering of X-ray photons. Scattering occurs when photons hit the electrons of the atoms inside the examined material. [21] As scattering occurs in every direction, it can be thought that a new spherical wave arises from every atom. Those new waves interfere with each other and a diffraction pattern emerges if the atoms are arranged in a periodic structure like in crystalline material. In amorphous material diffraction patterns can not be observed. The ideal diffraction angles from crystalline material can be calculated by using the Bragg's law

$$n\lambda = 2dsin(\theta), \tag{7}$$

where n is an integer, which tells the order of the diffracted beam, λ is the wavelength of the photons, d is the distance between the diffraction planes and θ is half of the angle between the scattered and the incident wave. It can be envisioned, that crystalline material consists of diffraction planes which "reflect" the X-rays, when the Bragg's law is satisfied. Diffraction planes are equivalent to the crystal planes with the exception that the set of diffraction planes doesn't include all the crystal planes because some of the crystal planes diffract radiation inside the crystal. [21]

XRR measurement can be used to examine the properties of thin films. With XRR the film thickness, roughness and electron density can be characterized. Unlike XRD, XRR is based on the reflection of X-rays from the interfaces between layers. The measured intensity of the reflected beam depends on the thicknesses, electron densities and the roughnesses of the surrounding films. The effect of every interface must be considered because the reflection from interfaces which are deeper in the sample affect the measured intensity. [20]

The XRR measurement starts at very small incident angles and almost all of X-ray radiation is reflected from the topmost interface. When the incident angle is increased the X-rays start to penetrate into the sample and the measured intensity starts to decay and oscillate as a function of the incident angle. The oscillation is due to the properties of films deeper in the sample. The range of measurement is usually just a few degrees due to the rapid decay of signal to noise ratio. [20]

The samples were studied with Philips X'Pert Pro, which is capable of performing both XRD and XRR measurements. The XRR measurements were used to characterize the film thicknesses of the AlN films and the XRD measurements were used to study the crystallinity of the AlN films. The setup used in XRD measurements was the same which is typically used in powder diffraction measurements with the exception that the sample was not ground up as powder. The setup was chosen, because it was expected that the AlN films had poor crystallinity and with powder diffraction setup it is easier to to detect, if any crystallinity exists.

5.2 Atomic Force Microscope

Atomic force microscope (AFM) can be used to measure and create images of surface topography. In the measurement the sample is scanned with a sharp tip. The tip is moved on or very near the surface of the sample. The direction and amount of the force directed to the tip is affected by the distance of the tip and the sample. The tip is on a cantilever, which is illuminated with a laser beam. The laser beam is reflected from a mirror on top of the cantilever to a detector. The detector consists of four segments so it can measure the deflection of the cantilever. The deflection is kept constant with a feedback loop. The sample is lowered or lifted corresponding to the signal from the detector. The basic operating principle of AFM is illustrated in figure 10.
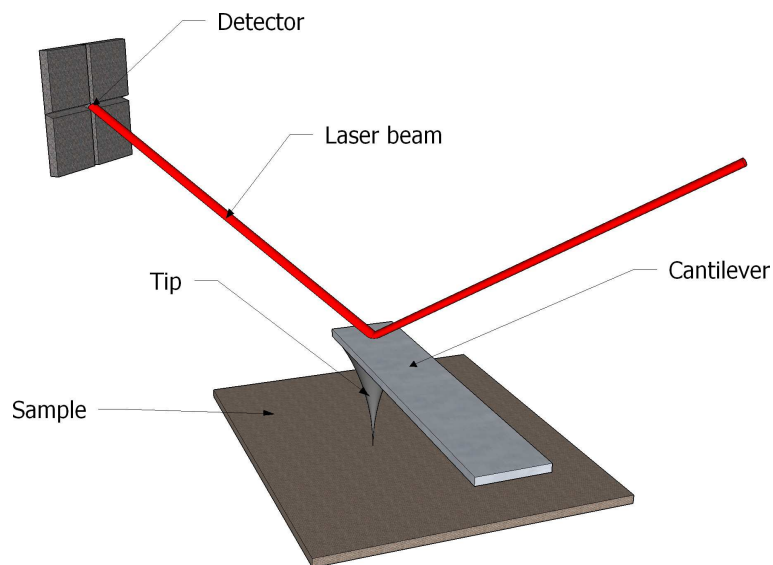
Figure 10: The basic operating principle of AFM. The sample is scanned with a sharp tip, which is on a cantilever. The deflection of the cantilever is measured with a laser beam.

AFM measurements can be executed in different modes. In contact mode the tip is in contact with the sample. Using contact mode atomic resolution can be achieved, but the tip can easily scratch the surface of the sample. Contact mode is suitable only for hard materials. In non-contact mode the tip moves near the surface of the sample instead of contacting it so it's better for softer samples. The distance of the tip and the surface of the sample is in the range of 1–10 nm. The force affecting the tip is the Van Der Waals force, which draws the tip towards the sample.

The forces affecting the tip are much smaller in the non-contact mode, hence the resolution is less than in contact mode. In non-contact mode the deflection of the cantilever or changes in resonance frequency of the cantilever can be measured. The resonance frequency changes when tip is brought closer to the sample due to change of effective spring constant of the cantilever is changed. Better resolution can be achieved by measuring the changes in resonance frequency instead of measuring the deflection. In semi-contact mode or tapping mode the tip is vibrating near the surface of the sample. The amplitude of the vibration is approximately 10 nm. In semi-contact mode the tip hits the surface of the sample, but it does not scratch it as much in contact mode. The topography data is measured in changes of the vibration amplitude.

For collecting data from the topography of samples made for this thesis NT-MDT nTegra AFM was used. The maximum measurement area was 14 μm $\times$ 14 μm, which was enough to determine the topography of the samples.

5.3   Scanning Electron Microscope

The wavelength of visible light limits the resolution of ordinary optical microscope. Electron microscopes utilize an electron beam instead of light to form an image from a sample. The wavelength of the electron beam is much smaller than the wavelength of visible light resulting in better resolution and a chance to get images from smaller details. Scanning electron microscope (SEM) sweeps the surface of the sample with an electron beam.

The basic operating principle of SEM is similar of a cathode ray tube. Electron beam is typically formed by heating up a tungsten filament and accelerating thermally emitted electrons with high voltage. The acceleration voltage typically ranges from 5 kV to 20 kV. The beam is focused to a small dot with magnetic lenses. The beam is scanned on the sample surface with scanning coils. As the beam hits the surface, it creates high-energy backscattered electrons due to elastic collisions and low-energy secondary electrons due to inelastic collisions. The image is typically formed with either of these. A schematic image of operating principle of SEM is shown in figure 11.

The surface of the examined sample should be conductive or coated with conductive material, *e.g.*, gold. Insulating materials have the tendency to charge up when illuminated with an electron beam. In this work SEM was used to examine the surface topography and integrity of the films. The samples examined with SEM were not coated in order to keep the samples unaffected by the examination which limited the resolution of the SEM images. The SEM was also used to examine the GaN films grown with MOVPE. GaN is conductive enough to achieve reasonably good images, so no coating was needed.

Two SEMs was used in this research. For examining the integrity of the AlN films Hitachi Tabletop TM-1000 was used. TM-1000 utilizes backscattered electrons to form image. For examining the GaN films Zeiss DSM-950 was used. DSM-950 forms image with secondary electron detector. The TM-1000 has the maximum magnification of 10000x and DSM-950 that of 300000x.
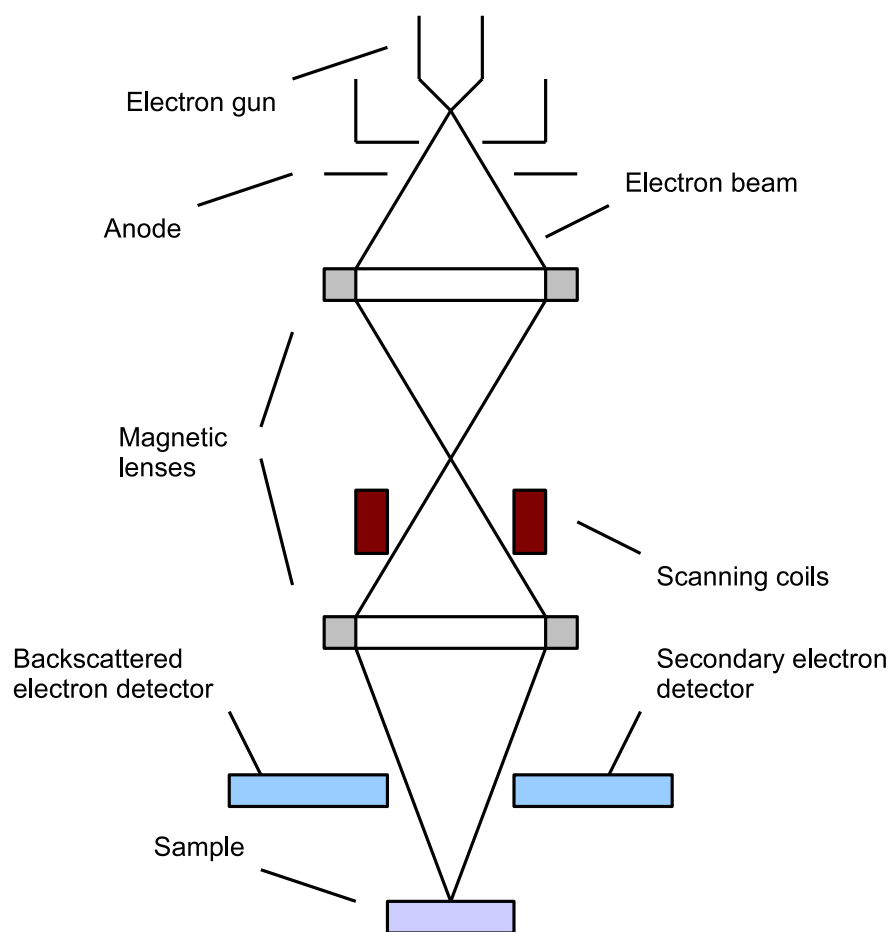
Figure 11: Schematic figure of the basic operating principle of SEM. An electron gun creates an electron beam, which is accelerated with high voltage. The beam is focused to a dot with magnetic lenses. Scanning coils are used to make the beam to scan the surface of the sample. SEM image can be formed with backscattered electrons or secondary electrons.

5.4 Ellipsometer

Ellipsometric measurement is based on measuring the state of polarization of light. The name ellipsometry stems from elliptic polarization. Ellipsometry is widely used to measure the thickness of dielectric thin films on absorbing substrates. It can also be used to determine optical constants of the measured films or substrates.

Light travels in transverse electromagnetic waves. All transverse waves are polarized even though natural light is called unpolarized light, which is actually a random mixture of linearly polarized waves. Circular polarization can be seen as a superposition of two linearly polarized equal-amplitude waves, which are perpendicular to each other and have a phase difference of a quarter of a wavelength. If the phase difference is other than a quarter of the wavelength or the amplitude of the waves is different, the polarization becomes elliptic. [10] If we consider transverse electric (TE) polarized wave propagating in z-direction in a right-handed cartesian coordinate system, we can denote the electric field in vector form

$$\vec{E}(t) = \left[\begin{array}{c} E_x(t) \\ E_y(t) \end{array} \right] = Re \left\{ \left[\begin{array}{c} Xe^{i\Delta} \\ Y \end{array} \right] e^{i\omega(t-t_0)} \right\}, \tag{8}$$

where X and Y are the amplitudes of electric field in corresponding axes and Δ is the phase difference between the x- and y-components. The intuitive choice for x- and y-axis for incident light is parallel and perpendicular to the plane of incidence, *i.e.*, p- and s-component, respectively. The plane of incidence is defined as a plane spanned by the surface normal and the propagation vector of the incident wave. The letter s stems from german word senkrecht, which means vertical.

Reflection polarizes light. When electromagnetic waves reflect, the electric-field component perpendicular to the plane of incidence is reflected more strongly than the component parallel to the plane of incidence. Thus, both the refracted and the reflected wave become partially polarized. When the incident angle is such that the reflected and refracted waves are perpendicular to each other, the reflected wave becomes completely polarized and the refracted wave partially polarized. Such an angle is called the polarizing angle. The relationship between the polarizing angle and refractive indices is called Brewster's law for polarizing angle

$$tan\theta_p = \frac{n_b}{n_a}, \tag{9}$$

where θ_p is the polarizing angle, n_b and n_a are the refractive indices of the materials. Brewster's law can be derived from the Maxwell's equations. [10]

In the measurement the sample is illuminated with a laser beam. The incident angle of the beam is fixed for each measurement. The polarization and the phase of the reflected beam are changed due to the properties of the measured film. In an ellipsometric measurement the measured values are so called ellipsometric angles Δ and Ψ. The angle Ψ is determined from the amplitudes of the p- and s-components by

$$tan(\Psi) = \frac{X}{Y}, \tag{10}$$

where X and Y are the amplitudes of p- and s-components. The reflection coefficients for p- and s-components are not measurable as they are, but the complex reflection ratio ρ is. The reflection ratio is defined as

$$\rho = \frac{R_p}{R_s} = tan(\Psi)e^{i\Delta}, \tag{11}$$

where R_p and R_s are the reflection coefficients for p- and s-components and i is the imaginary unit. As can be seen, it is not necessary to make absolute intensity or phase measurements. [22]

The ellipsometric angles Ψ and Δ are sensitive to composition, microstructure and optical constants of the sample in addition to layer thickness. Hence, it is good to obtain multiple data sets in the measurement. In a conventional ellipsometer the wavelength of the laser is fixed, but a spectroscopic ellipsometer (SE) uses multiple wavelengths to obtain more data from the measured sample. One can also measure using different incident angles. [22]

In principle there is no limitation for the measured film thickness. However, the model used to fit the data sets it's own limitations. In very thin films the problems arise from the assumptions for uniform optical properties and sharp planar interfaces. Also the equations used are based on macroscopic Maxwell's equations. On thick layers the interpretation of the measurement becomes difficult due to interference between the beam reflected on the surface and the beam reflected on the interface of the substrate and the measured film. The interference causes cyclic behavior of Ψ and Δ. If the film is thicker than the cycle thickness, one must know the thickness within one cycle. The cycle can be calculated from

$$d = \frac{\lambda}{2\sqrt{n_1^2 - sin^2(\theta)}}, \tag{12}$$

where d is the film thickness, λ is the used wavelength, n_1 refractive index of the film and θ is the incident angle. [22] *E.g.*, if one measures a film with a refractive index of 1.8 with a wavelength spectrum ranging from 800 to 1700 nm and performs the measurements with an incident angle 70°, the cycle thickness varies from 250 to 550 nm as a function of wavelength. These values are close to the setup used in this research. As the thickness of the grown AlN film falls below the cycle thickness, the cyclic behavior of the ellipsometric angles is not a problem.

Typical model used in ellipsometric analysis assumes that the measured film is transparent and the substrate absorbs the light refracted into the substrate. The measured film can be ideal or one can add losses in the analysis. If the assumptions are not valid, the fitted model is not accurate and can be completely useless.

Sentech Instruments SE 805 spectroscopic ellipsometer was used to obtain information about film thicknesses and refractive indices of the AlN films. The used

wavelength spectrum ranged from 800 to 1700 nm and the measurements were performed with the incident angles of 50, 60 and 70°.

6 Experimental

The experimental work began with PEALD growth of AlN on silicon followed by thermal annealing. The films were characterized before and after the annealing. Finally a GaN film was grown with MOVPE and characterized. As described in the previous chapters the orientations of the silicon substrate affects on the properties of the grown films. Therefore silicon wafers with different orientations were tested in this work. Silicon substrates used for this thesis were (1 0 0)-, (1 1 0)- and (1 1 1)-oriented wafers.

6.1 Deposition of Aluminum Nitride

The silicon wafers used in this research were dipped in HF before depositing the AlN layer. The HF dip was performed to remove the native oxide and to achieve a hydrogen-terminated surface on the silicon wafers. To obtain the desired layer thickness of 200 nm of AlN 1800 cycles were needed in the PEALD process. The calculation was based on previous film growth experiments. All used silicon substrates were put inside the chamber at the same run to obtain comparable AlN layers. The growth temperature of the process was 200 °C which is the maximum growth temperature of the used ALD system.

6.2 Thermal Annealing

Tuning of the PID of the RTP was done with trial and error method. Only one PID table was specified for the RTP. Since the temperature ramps were steady and no significant overshoot occurred, no more than one PID table was needed. Nitrogen is usually used for annealing nitrides, but annealing done in RTP for this thesis was performed in argon atmosphere due to lack of mass flow controller in the nitrogen valve in the used RTP.

The first step in the recipes made for annealing was to pump the reaction chamber down to vacuum. After evacuating the chamber, 500 sccm of argon was flown for time period of 150 s. At this point the pressure inside the chamber was roughly 1100 mbar. During the rest of the process 50 sccm of argon was flown through the chamber to keep the pressure inside the chamber somewhat constant. Heating the chamber was started with a constant heating power to achieve sufficient temperature for getting readout from the pyrometer. Then the process was switched to pyrometer control.

The samples were annealed at 600, 800 and 1000 °C. The ramp up rate was set to $10\frac{°C}{s}$. After the ramp up the temperature was kept steady for 90 s. The ramp down rate was limited in $10\frac{°C}{s}$ until the setpoint of 400 °C was reached. After the process ended, the chamber was purged with nitrogen. One example of used annealing process is shown in figure 12. In this figure pressure, measured temperature and setpoint is drawn as a function of time.
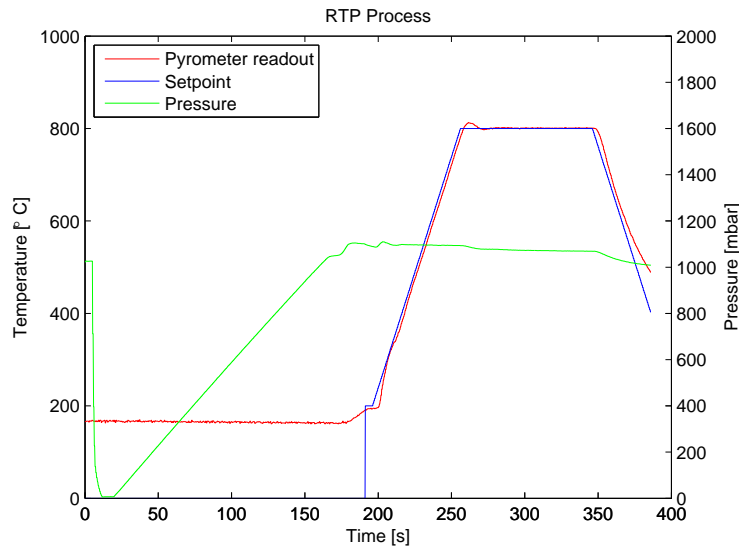
Figure 12: Example of a performed RTA process. At the beginning the chamber was pumped down to vacuum and filled with argon. Then, for a short period of time the RTP was driven with constant power to obtain temperature readout from the pyrometer. The setpoint was increased with a constant ramp up rate until the desired temperature was achieved. The set point was kept at steady state for 90 s. Ramp down rate was limited to equivalent to ramp up rate until the setpoint of 400 °C. After the process the chamber was purged with nitrogen.

In addition to RTP a conventional tube furnace (CTF) was used. CTFs have relatively low temperature ramp rates. Also it is possible to anneal for reasonably long times. The purpose of using a CTF was to give contrast to RTA's high ramp rates and short annealing times. The ramp up rate in the tube furnace is approximately $1\frac{°C}{s}$ and the annealing time varied from 30 to 60 min. Annealing in the CTF was performed in a nitrogen environment.

6.3 GaN Growth on AlN Layer

Prior to MOVPE process the samples were cleaned in acetone dip in ultrasonic drain followed by a isopropanol dip. After this the sample was rinsed in deionized water and blown dry with nitrogen.

In GaN growth a typical two-step process was used, which consists of growing the low temperature nucleation layer and of the high temperature growth. In addition, high temperature growth of GaN without a low temperature nucleation layer was tested. The approximated real temperatures of the two-step process temperatures were 550 °C and 1000 °C in low and high temperature growth, respectively. The approximated real growth temperature of the single-step growth ranged from 700 to 1000 °C.

During the growth of the nucleation layer in the two-step process ammonia and

TMGa were flown to the reaction chamber for 125 s after which the temperature was ramped up to the actual growth temperature. During the ramp up TMGa flow was set to by-pass. The high temperature growth lasted for 2000 s. In the single-step process the high temperature growth lasted for 2000 s as well. After the samples were characterized, the growth was continued for both type of samples for 5000 s. The samples were again cleaned in a aforementioned way prior continuing the growth.

7 Results and Discussion

The samples were studied with several characterization instruments to obtain information about the effects of the annealing. The following chapter covers the results and discussion about measurements. The characteristics studied were film thickness, crystallinity and surface topography.

7.1 Film Thickness

Film thicknesses were measured to see whether the annealing caused decomposition of the AlN films. Also by measuring the films with an ellipsometer, information about the refractive indices of the annealed films are obtained. The refractive index of amorphous AlN is lower than that of crystalline AlN.

The AlN films grown on silicon were conform with the exception of the film grown on the (1 1 1)-oriented substrate. This was determined by the coloration of the grown films. The (1 1 1)-oriented substrate moved during the growth process too close to the wall of the reactor chamber. Thus, the film grew less than expected on the edge closest to the reactor chamber wall. This could be seen as gradient of coloration of the grown film.

The sample thicknesses were studied with X-ray reflectivity (XRR) and spectroscopic ellipsometer (SE). The determination of the thickness of the AlN layer was found to be more difficult than expected. There were problems in both XRR and SE measurements. Due to the reasonably thick layers the fringes in XRR measurements were reasonably small. There was some distortion in the measured XRR data, which had a huge effect on the small fringes. The distortion was believed to originate from the curvature of the samples. It is also possible that the cracks in the AlN films distorted the XRR measurement. Hence, the fitting of the simulated films to the measured data was difficult.

Due to the transparency of silicon for wavelengths of over 1000 nm the ellipsometric measurements were also found to be difficult. The model used for fitting the measurement data assumes that the beam refracted to the substrate is absorbed. The used silicon (1 1 0)- and (1 1 1)-oriented substrates were double side polished wafers and the bottom side of the wafers acts as a mirror. Hence, the data collected from the transparent region of silicon can be more or less random depending on the bottom side smoothness. Data collected only from wavelength spectra $800 - 900$ nm was used in fitting the film parameters and the thickness information based on these measurements is not as accurate as possible. The (1 0 0)-oriented silicon wafers were polished only on one side. The rough surface on the bottom side scatters the refracted light and the assumption in the model can be considered as valid and the whole measured wavelength spectra was used. The used wavelength spectra ranged from 800 to 1700 nm.

The measured thicknesses of AlN films grown on (1 0 0)-oriented silicon substrate are plotted in figure 13. The shown thicknesses are measured with SE and XRR.

Also the thicknesses of the samples annealed in conventional tube furnace (CTF) are shown in this figure. As can be seen, the thickness slightly decreases as a function of temperature. The thicknesses of the samples annealed in the tube furnace and in the RTP have no significant differences. The rest of the measured thicknesses are shown in table 1.
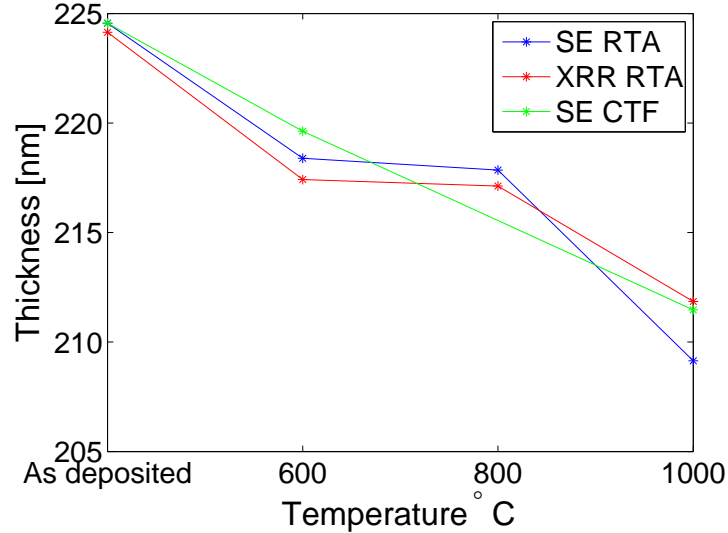

Figure 13: Thicknesses of annealed and as-deposited AlN films grown on (1 0 0)-oriented silicon substrate. Points measured with SE and XRR are shown in blue and red, respectively. For comparison the thicknesses of the samples annealed in the CTF are shown with green. The samples annealed in the CTF were measured with SE only.

| | | Measured film thickness [nm] | | | | | |
| | | (1 0 0) | | (1 1 0) | | (1 1 1) | |
Process	Temperature	SE	XRR	SE	XRR	SE	XRR
-	-	225	224	218	222	219	139
	600 °C	218	217	218	218	232	219
RTA	800 °C	218	217	213	211	215	214
	1000 °C	209	212	207	212	203	210
CTF	600 °C	220	-	218	-	218	-
	1000 °C	211	-	209	-	207	-

Table 1: The measured film thicknesses of AlN films grown on (1 0 0)-, (1 1 0)- and (1 1 1)-oriented silicon substrates. The samples were annealed in RTP and CTF and measured with SE and XRR.

The quality of both XRR and SE fittings can be estimated from figure 14. The data presented in figure is taken from as-deposited films. As can be seen, the SE measurement of the sample grown on (1 0 0)-oriented silicon has a good fit in the whole wavelength spectra used in the measurement. The ellipsometric angles

measured from the samples grown on (1 1 0)- and (1 1 1)-oriented silicon are useless on the transparent region of silicon, *i.e.*, at wavelengths of over 1000 nm. The effect of silicon becoming transparent can be easily seen from the measurement data. The rest of the XRR and SE fittings used in the thickness analysis is found from the appendices A1 – A3 and A4 – A6, respectively.
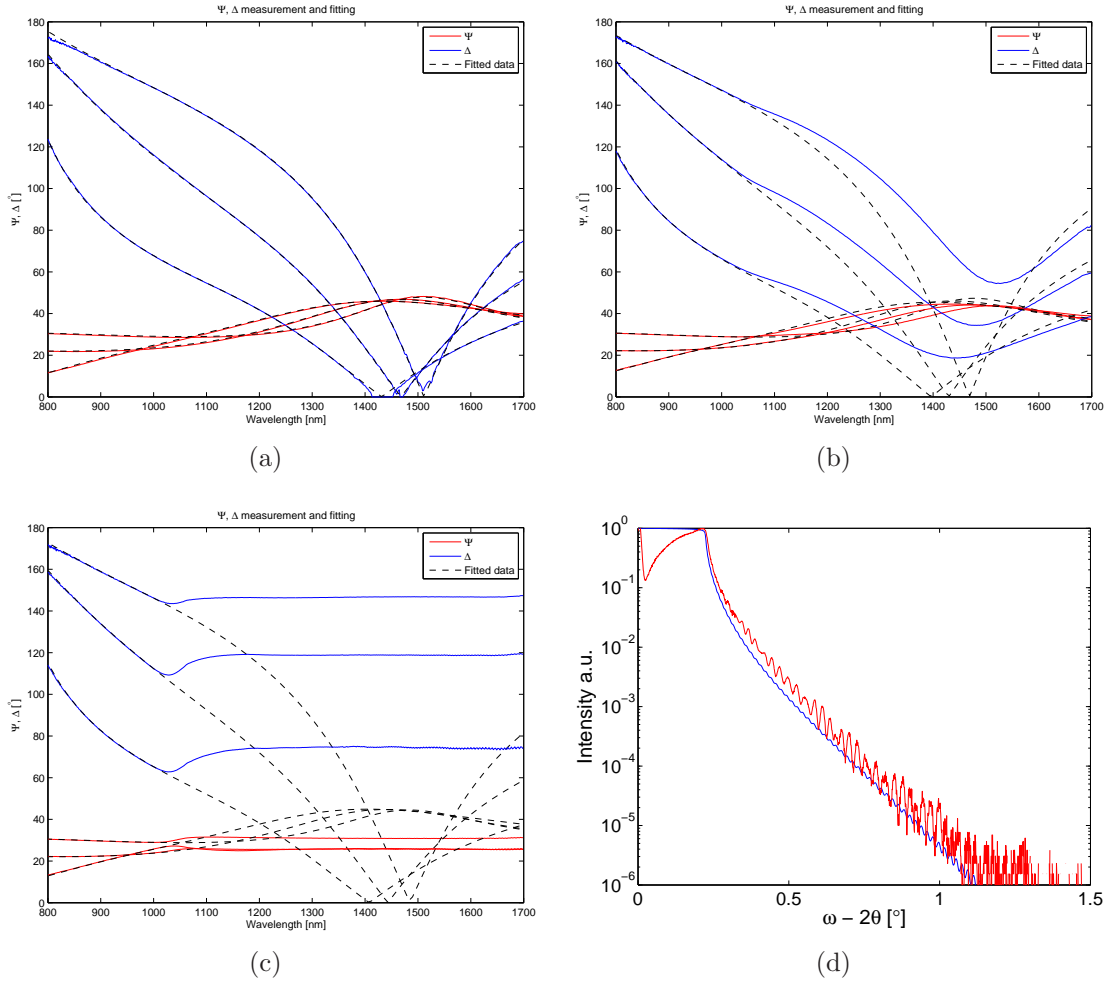

(a)

(b)

(c)

(d)

Figure 14: SE measurements of as-deposited AlN films grown on (a) (1 0 0)-, (a) (1 1 0)- and (c) (1 1 1)-oriented silicon substrates and corresponding fitted models. The measured Ψ is drawn in red and Δ in blue. The fitted Ψ and Δ are shown in black dashed line. From (b) and (c) the effect of silicon transparency in the wavelengths of over 1000 nm can be clearly seen. (d) XRR measurement and simulation of as-deposited film grown on (1 0 0)-oriented silicon substrate. The measured intensity is drawn with red and the simulated curve with blue.

The refractive index can be calculated from the SE measurement with the same fitting procedure. Calculated refractive indices are presented in figure 15. As can be seen the refractive index decreases in the annealing process. The refractive index had decreased most in the samples, which were annealed at 1000 °C in the CTF. The decrease of the refractive index implies that no crystallization has occurred.

The refractive index of single crystal AlN ranges from 2.1 to 2.2, polycrystalline film from 1.9 to 2.1 and amorphous AlN from 1.8 to 1.9 [6].

The annealed films were measured to be thinner than the as-deposited films. It seems that some decomposition occurs, but it is in relatively small scale. The annealing time does not seem to affect the decomposition, but the refractive index seems to decrease as a function of annealing time. It can also be due to the the annealing environment. The annealing in the RTP was performed in significantly cleaner environment than the annealing in the CTF. Based on the measurement of the refractive index, the as-grown films were amorphous and the minor change of refractive index by annealing indicates that no crystallization occurs.
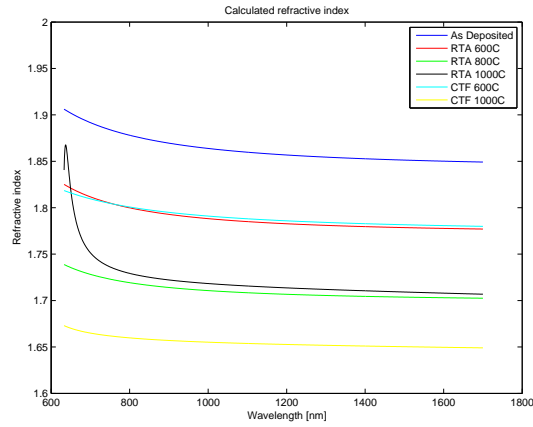
(a)
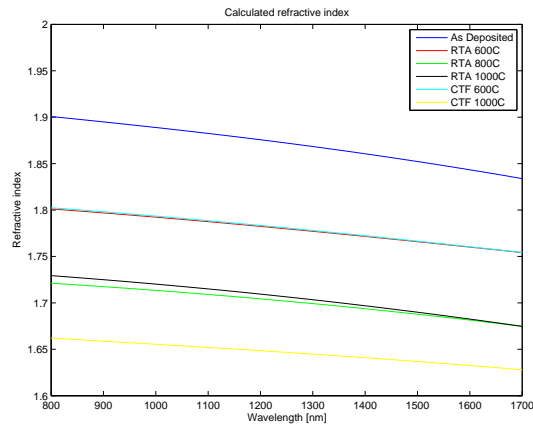
(b)
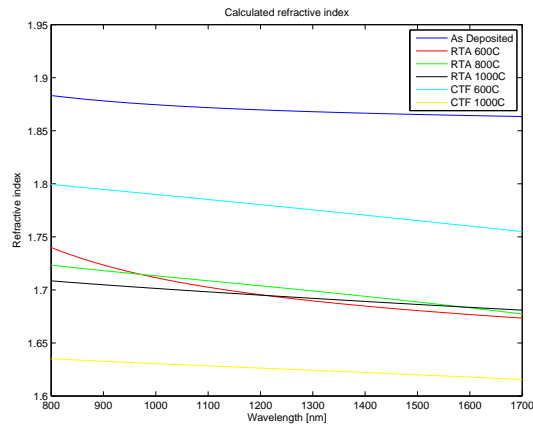
(c)

Figure 15: Calculated refractive indices of annealed AlN grown on (a) (1 0 0)-, (b) (1 1 0)- and (c) (1 1 1)-oriented substrates. The refractive index decreases as a function of temperature. Also longer annealing time seems to reduce the refractive index.

7.2 Topography

Optical microscope and SEM were used to examine the surface integrity of the samples. The as-deposited films were found to be crack-free and conformal. Cracks were found in all annealed samples and the number of cracks increased as a function of temperature as can be seen in figure 16. The orientation of the substrate had no significant effect on the crack density. The samples annealed in tube furnace had less cracks than the ones annealed in RTP indicating that the temperature ramp rate has a significant effect on the cracking.

The cracks found in films grown on (1 1 1)-oriented silicon substrate were more severe than the ones found in films grown on (1 0 0)- and (1 1 0)-oriented substrates. As can be seen in figure 17 the cracks are wider in the film grown on (1 1 1)-oriented wafer. The samples shown in this figure are annealed at 1000 °C in RTP. There is no noticeable difference between the films grown on (1 0 0)- and (1 1 0)-oriented wafers.

To obtain information about the topography of the surfaces of the samples an AFM was used. The studied films had very smooth surfaces before and after the annealing. It seemed that the annealing did not affect the surface roughness. This can be seen in topography images shown in figure 18. The rest of the measured AFM images are shown in appendices B1 and B2.

As the coloration of 2-dimensional AFM images can be misleading cross section profiles were taken from the measured images. The cross section profiles of films grown on (1 1 1)-oriented substrate are shown in figure 19. The surface of the AlN film is smooth and annealing seems to have no effect on topography excluding the cracks formed during annealing. The films have only a few nanometers of variance in the surface.

When thin films are annealed, thermal stress is induced to the annealed film. If the thermal stress increases over the breaking strength of the film, it relaxes by cracking. The cracks found were most likely formed due to tensile stress during cooling down from the annealing temperature. The recipe used in RTP treatment was stopped, when the setpoint was 400 °C. The temperature of the sample was still approximately 500 °C, when the purge valve of the RTP was opened. This induced great amount of thermal stress in a short period of time resulting in the cracking of the film. The cooling down of the tube furnace took several hours, hence the thermal shock was not so violent. The reason, why films grown on (1 1 1)-oriented silicon wafers had wider cracks, is yet unknown.
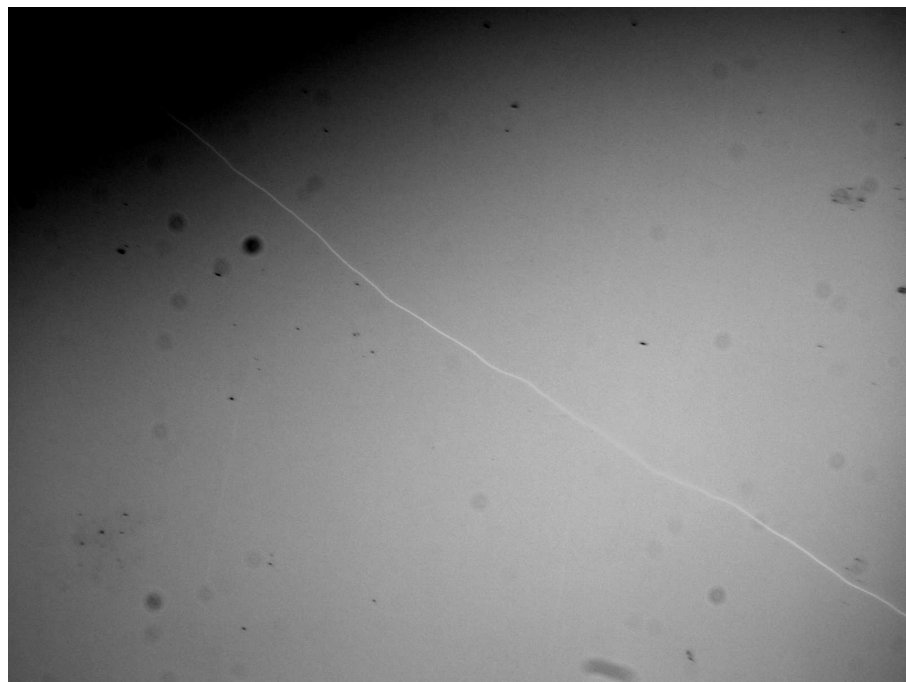
(a)
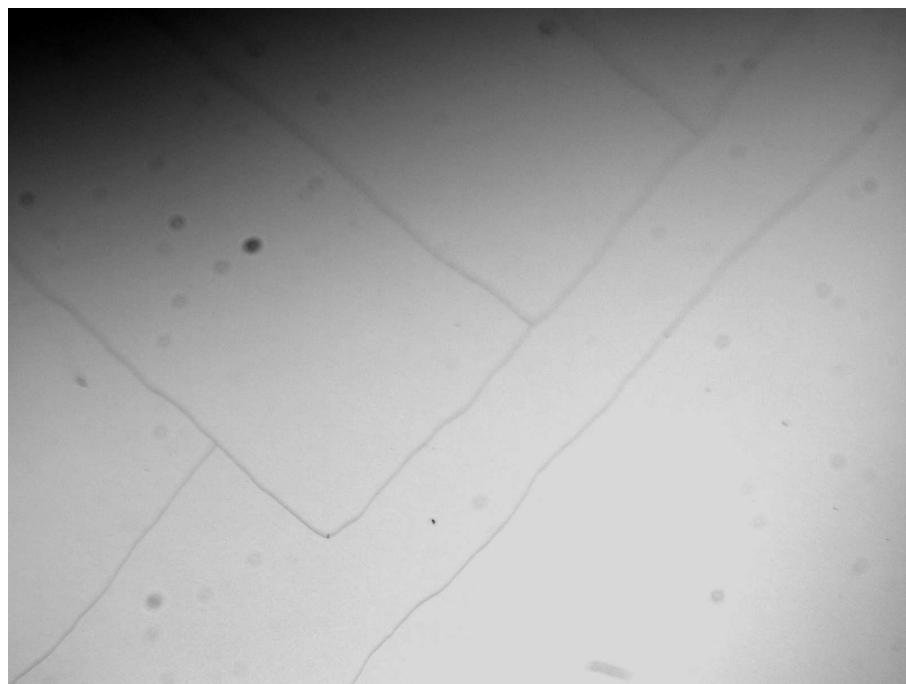
(b)

Figure 16: Optical microscope images taken from AlN films grown on (1 0 0)-oriented silicon substrate. The samples were annealed in RTP at (a) 600 °C and (b) 1000 °C. The density of cracks increases as a function of annealing temperature.
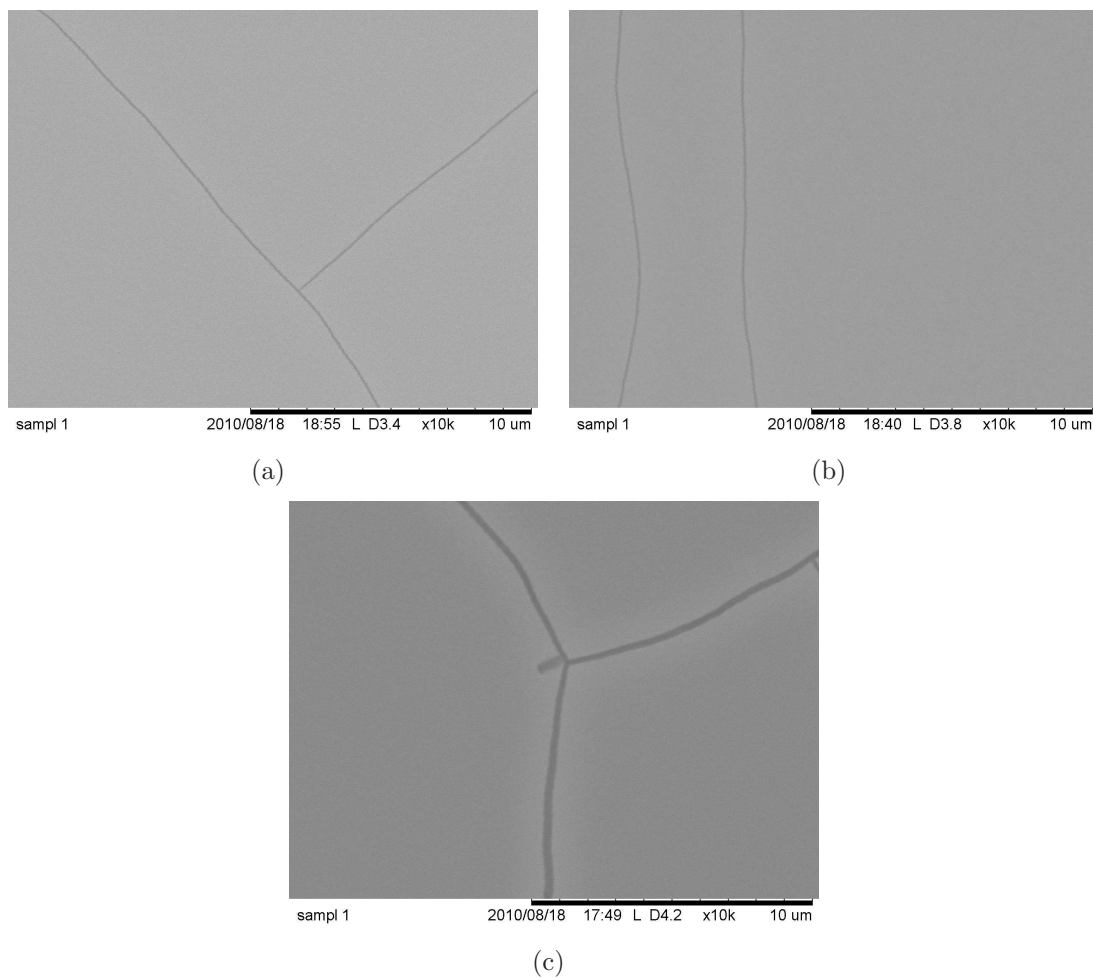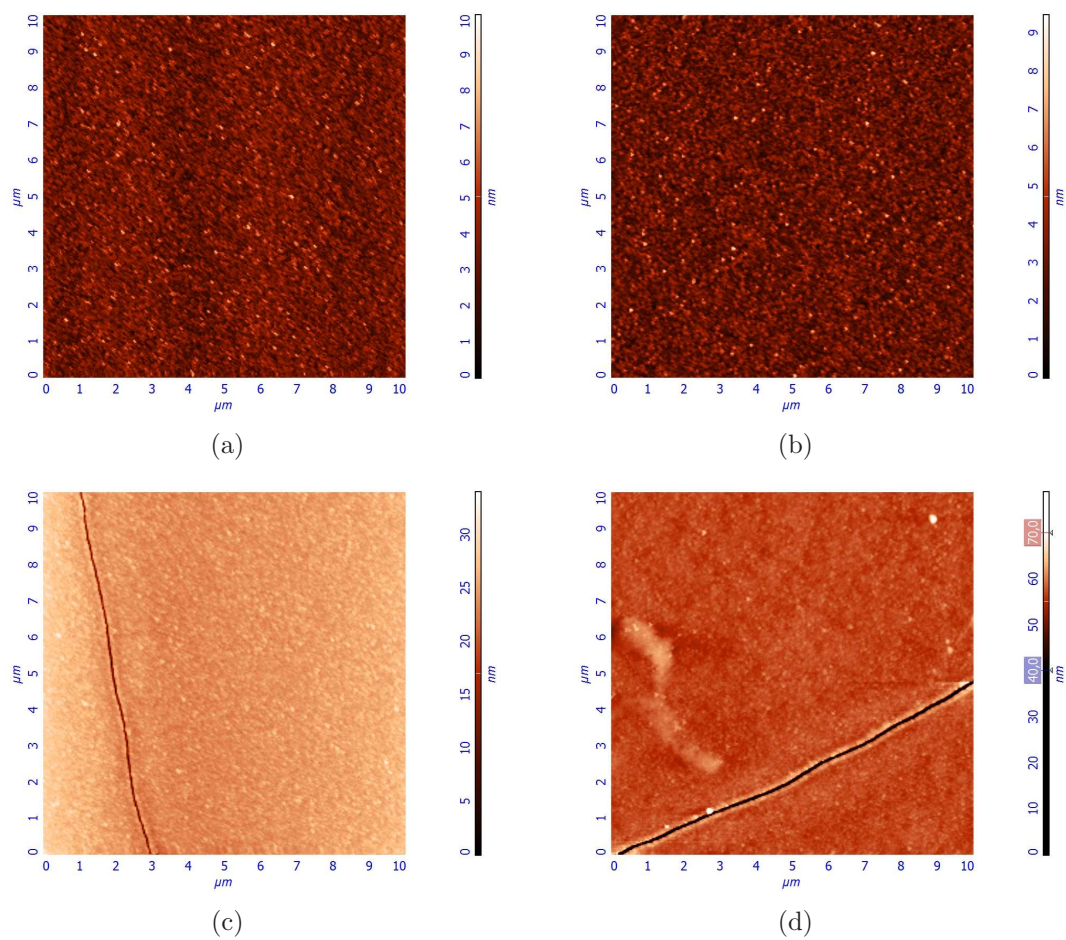
Figure 17: SEM images from annealed AlN film grown on (a) (1 0 0)-, (b) (1 1 0)- and (c) (1 1 1)-oriented silicon wafer. The films were annealed at 1000 °C for 90 s. The cracks found on AlN films grown on (1 1 1)-oriented silicon wafer were found to be wider than ones found in films grown on (1 0 0)- and (1 1 0)-oriented substrates.

Figure 18: AFM images of AlN films grown on (1 1 1)-oriented silicon (a) as deposited and after annealing at (b) 600 °C, (c) 800 °C and (d) 1000 °C for 90 s. As can be seen the surface is very smooth, only a few nanometers of surface roughness. Cracks created by thermal stress can be seen in (c) and (d). The coloration has been altered in (d) to obtain a better contrast in the image.
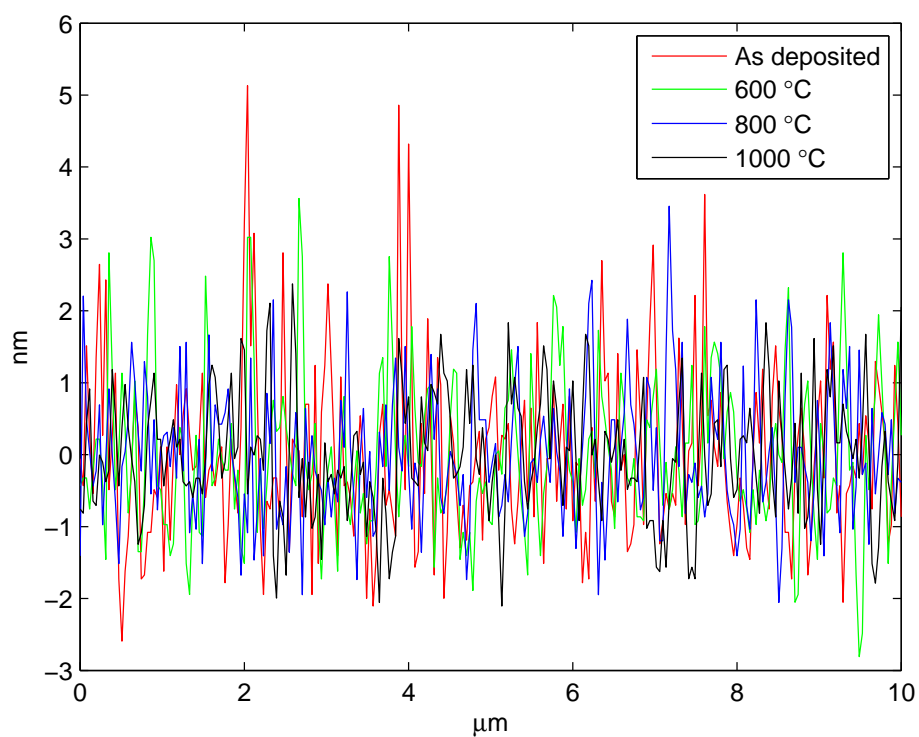
Figure 19: Cross section profiles of films grown on (1 1 1)-oriented substrate and annealed in RTP. The surface of the AlN film is smooth and annealing seems to have no effect on topography excluding the cracks formed during annealing.

7.3 Crystallinity

The setup used to measure crystallinity was the same used for powder XRD measurement with the exception that the sample was not ground up to powder. The reason behind using this setup was to find any crystallinity if any occurred. The measurement setup had a few drawbacks. The smallest measured samples were smaller than the irradiated area. Hence the sample holder was also illuminated in the measurement. This could be seen as extra diffraction peaks. The problem was solved by inserting a glass plate between the measured sample and the sample holder.

The performed XRD measurements were reasonably long symmetrical ω-2θ scans. The ω angle ranged from 13.5° to 27° with a stepsize of 0.003°. Each step had an integration time of 0.2 s. ω-2θ scans performed to AlN films grown on (1 0 0)-oriented silicon substrates are shown in figure 20. As can be seen from the XRD measurements there are two diffraction peaks. Both of them originate from the silicon substrate. First one is the diffraction peak of (2 0 0)-plane and the second one (4 0 0)-plane. All the XRD measurements are similar, with the difference of angles in which the diffraction peaks of the substrate are found. No diffraction peaks of AlN were found, thus the deposited AlN layer can be concluded to be amorphous and annealing had no crystallizing effect.

X. Liu *et al.* have realized polycrystalline AlN films deposited with PEALD using growth temperatures of 370 – 470 °C [11]. The samples in this work were grown at 200 °C, which is the maximum growth temperature of the used ALD. The low growth temperature results in amorphous AlN films, and it seems that they cannot be crystallized by thermal annealing. Rest of the XRD measurements can be found in appendices C1 and C2.
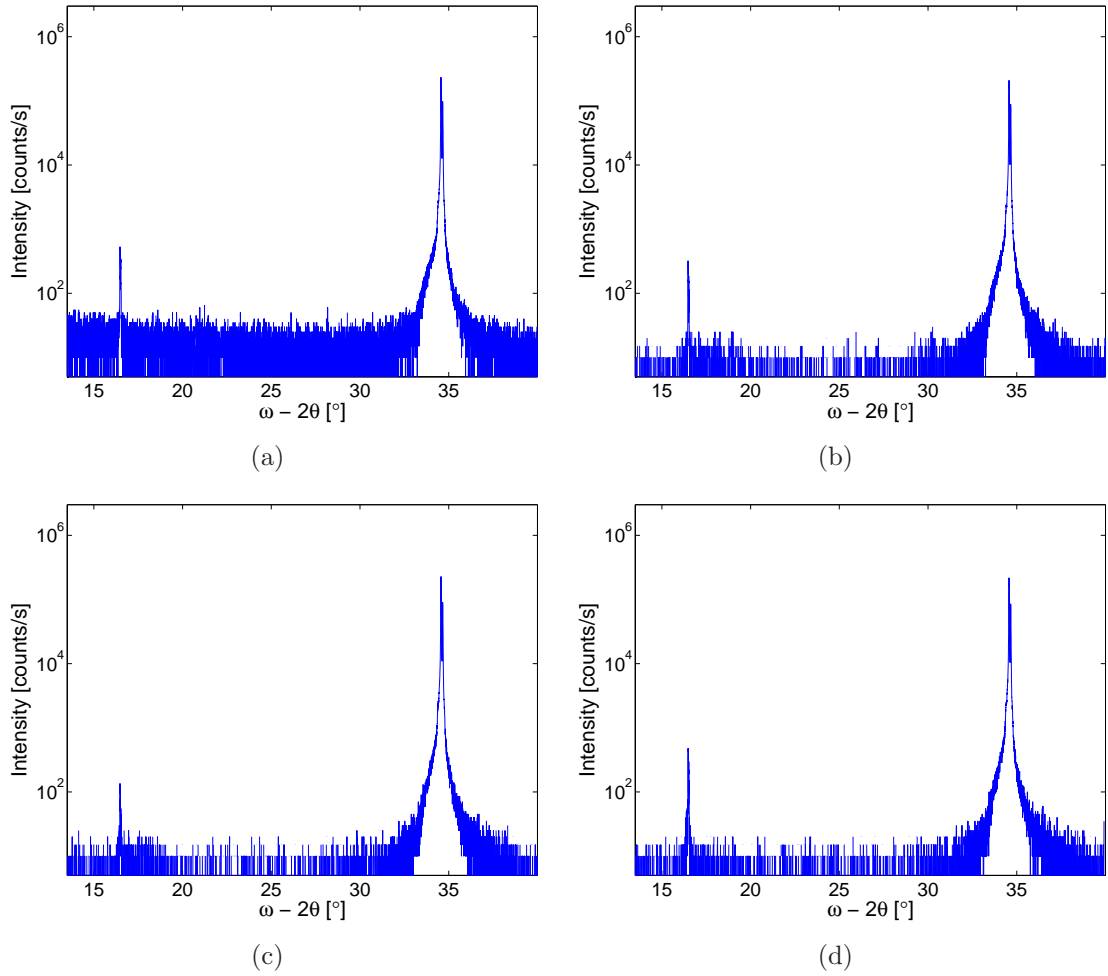
Figure 20: ω-2θ-scans of samples grown on (1 0 0)-oriented silicon substrate (a) as deposited and annealed at (b) 600 °C, (c) 800 °C and (d) 1000 °C. Two diffraction peaks were found in the measurements. These peaks originate from the diffraction planes (2 0 0) and (4 0 0) of the silicon substrate. No diffraction from the AlN films was detected.

7.4 GaN on AlN Coated Silicon

Even though the deposited AlN film was amorphous and annealing did not seem to commence crystallization, the growth of GaN was experimented on the AlN films. As the annealing of the AlN films induced cracks to the AlN film and no crystallizing effect of the annealing was observed, the GaN growth with MOVPE was performed on untreated AlN films. It was better to use samples that were processed as little as possible to obtain the most clean and best quality substrate for GaN.

The readout from the relflectometer and the pyrometer of the two-step growth of GaN is shown in figure 21. In the beginning of the process the temperature was ramped up to the growth temperature of the nucleation layer and the reflectance increased due to yet unknown surface reactions. One can see a half period oscillation
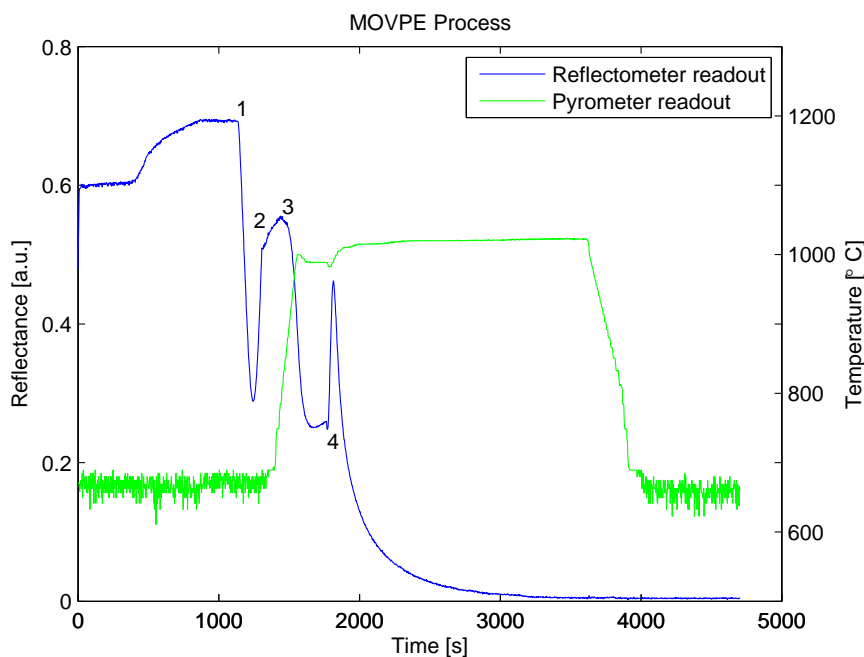
Figure 21: Reflectance and pyrometer readout during a two-step MOVPE process. The key points in the process are marked in the figure. (1) The beginning of the low temperature growth. (2) The temperature starts to increase. (3) A notch is seen, as the nucleation layer starts to decompose and recrystallize. (4) The beginning of the high temperature growth.

during the low temperature growth of the nucleation layer. This was not expected, since during growth of GaN on sapphire, the reflectance increases only a bit and then saturates. As the temperature was ramped up to the actual growth temperature, a typical notch in reflectance is seen at around 850 °C. The notch originates from the partial decomposition and recrystallization of the low temperature nucleation layer. As the high temperature growth began, the reflectance increased followed by rapid decay of the reflectance. In a typical GaN growth on sapphire, the reflectance should increase after a moment and start to oscillate. Instead the reflectance readout continued to decrease indicating that the surface roughness increases.

From SEM images the enormous surface roughness can be seen. In figure 22 cross section of GaN film grown 2000 s with low temperature nucleation layer is shown. The islands do not coalesce even with very long growth time. SEM images from sample grown for 2000 s without a low temperature nucleation layer and the same sample after continuing the growth for 5000 s is shown in figure 23. At first large crystals are formed on the surface of the sample. As can be seen in the image crystals grown on the AlN film have no preference in orientation, which prevents the crystals from coalescing even with very long growth time.
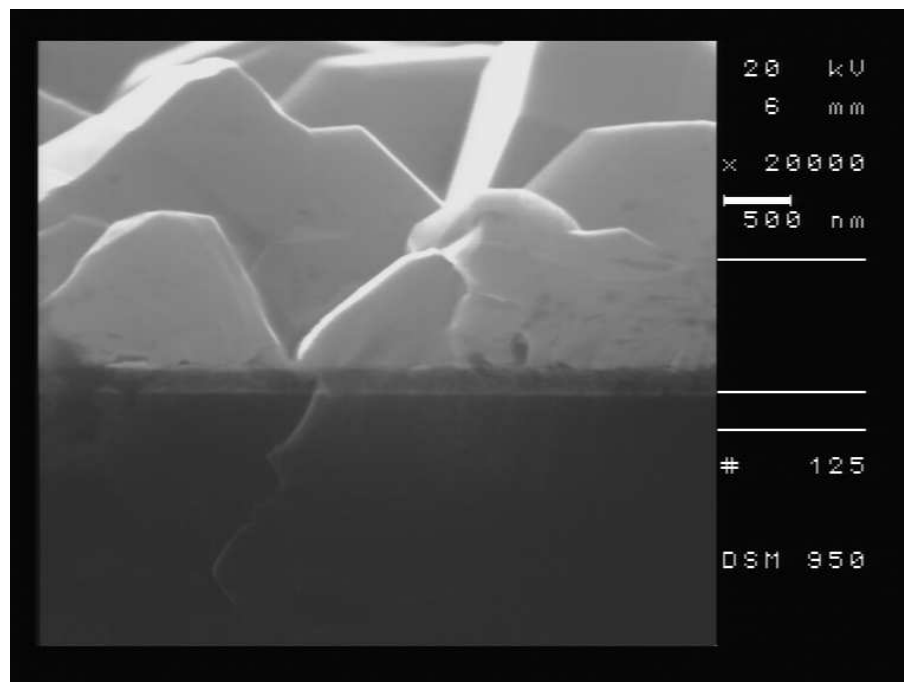
Figure 22: SEM cross section image of a GaN film grown on AlN by two-step method. Roughly 200 nm thick AlN film can be seen between GaN and silicon. The deposited GaN is hardly a film and it is extremely rough.

The grown GaN layer resulted in a very rough polycrystalline film with large size crystals with mixed orientations, regardless of whether the growth was one or two-step process. As the AlN film was amorphous, it did not give any preference to the orientation of the growing GaN layer. Hence, the crystals formed during the growth were randomly oriented. As the growth proceeded, the islands did not coalesce and uniform single crystal layer was not obtained.
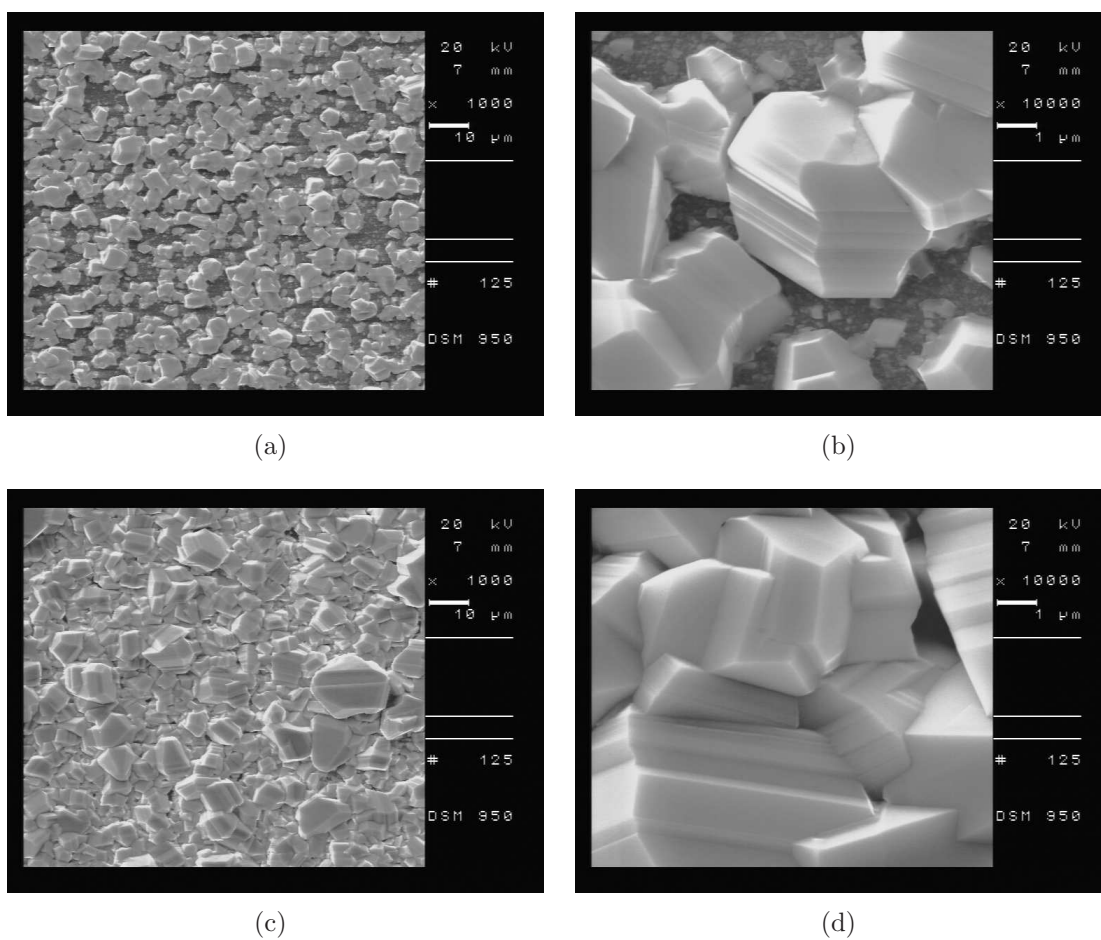
Figure 23: SEM images of GaN film grown for 2000 s with a magnification of (a) 1000x and (b) 10000x. GaN film after 5000 s of regrowth with a magnification of (c) 1000x and (d) 10000x. The growth temperature was 1000 °C.

8 Conclusions

The goal of this thesis was to research the effects of thermal annealing on AlN grown by PEALD on silicon substrate. The characteristics studied were film thickness, topography, crystallinity and refractive index. In addition GaN growth by MOVPE on PEALD grown AlN was tested. The reason of growing the GaN film was to study how PEALD grown AlN film on silicon could act as a substrate for GaN growth.

The deposition of AlN was performed on silicon wafers with different orientations. The used silicon substrates were (1 0 0)-, (1 1 0)- and (1 1 1)-oriented. 200 nm of AlN was deposited at 200 °C. The samples were annealed in a RTP and in a CTF. The annealing temperatures varied from 600 to 1000 °C. The annealed samples were characterized with different measurement equipment to obtain information about the annealed films. The growth of GaN was experimented with and without a low temperature nucleation layer.

AlN film deposited with PEALD in a temperature of 200 °C proved to be amorphous. According to research of X. Liu *et al.* the PEALD deposition of polycrystalline AlN film requires growth temperatures of over 370 °C [11]. The surface of the grown layer was very smooth and no cracks or pinholes were found. Thermal annealing did not cause crystallization in the AlN films. The refractive index seemed to decrease as a function of annealing temperature. Refractive index of the samples annealed in tube furnace for a long period of time was lower than the samples annealed in RTP indicating that also annealing time affects the refractive index. The surface of the AlN film remained very smooth after annealing with the exception of cracks, which were found in every annealed sample. The number of cracks increased as a function of temperature. The substrate orientation had no significant effect on the crack density, but the cracks found in films grown on (1 1 1)-oriented silicon were more severe. The samples annealed in the tube furnace had less cracks in the film indicating that the temperature ramp rate has a significant effect on the cracking. The film thickness slightly decreased as a function of annealing temperature. This is probably due to minor decomposition of the AlN film.

Even though the AlN films were amorphous GaN growth by MOVPE was experimented. The grown films were extremely rough and polycrystalline with reasonably large grains. The amorphous AlN layer did not give any preference for orientation of the GaN crystals grown, hence the grains formed on the AlN film were with mixed orientations.

References

[1] S. Nakamura and G. Fasol. *The Blue Laser Diode*. Springer, New York, 1997.

[2] H-Y Lee, X-Y Huang, and C-T Lee. Light output enhancement of gan-based roughened leds using bias-assisted photoelectrochemical etching method. *Journal of The Electrochemical Society*, 155(10):H707–H709, 2008.

[3] F. Reiher, A. Dadgar, J. Bläsing, M. Wieneke, M. Müller, A. Franke, L. Reissmann, J. Christen, and A. Krost. Ingan/gan ligh-emitting diodes on si(110) susbstrates grown by metal-organic vapour phase epitaxy. *Journal of Physics D: Applied Phisics*, 42:055107–1–4, 2009.

[4] B. Liu, J. Gao, K. M. Wu, and C. Liu. Preparation and rapid thermal annealing of aln thin films grown by molecular beam epitaxy. *Solid State Communications*, 149:715–717, 2009.

[5] J. Singh. *Semiconductor Optoelectronics: Physics and Technology*. McGraw-Hill, Inc., Singapore, 1995.

[6] H. Morkoc. *Handbook of Nitride Semiconductors and Devices Volume 1: Material Properties, Physics and Growth*. Wiley-VCH, Weinheim, 2008.

[7] R. Liu, F. A. Ponce, A. Dadgar, and A. Krost. Atomic arrangement at the aln/si (111) interface. *Applied Physics Letters*, 83(5):860–862, 2003.

[8] O. E. Contreras, F. Ruiz-Zepeda, A. Dadgar, A. Krost, and F. A. Ponce. Atomic arrangement at the aln/si (110) interface. *Applied Physics Express*, 1:061104–1–3, 2008.

[9] Y. J. Lee and S-W Kang. Growth of aluminum nitride thin films prepared by plasma-enhanced atomic layer deposition. *Thin Solid Films*, 446:227–231, 2004.

[10] H. D. Young and R. A. Freedman. *Sears and Zemansky's university physics: with modern physics*. Pearson Addison-Wesley, San Francisco, 2007.

[11] X. Liu, S. Ramanathan, E. Lee, and T. E. Seidel. Atomic layer deposition of aluminum nitride thin films from trimethyl aluminum (tma) and ammonia. *Material Research Society*, 811:D1.9.1–D1.9.6, 2004.

[12] J. P. Kar, G. Bose, and S. Tuli. Influence of rapid thermal annealing on morphological and electrical properties of rf sputtered aln films. *Materials Science in Semiconductor Processing*, 8:646–651, 2005.

[13] L. Vergara, J. Olivares, E. Iborra, M. Clement, A. Sanz-Hervás, and J. Sangrador. Effect of rapid thermal annealing on the crystal quality and the piezoelectric response of polycrystalline aln films. *Thin Solid Films*, 515:1814–1818, 2006.

[14] M. Bosund. Galliumarsenidipinnan passivointi. Master's thesis, Helsinki University of Technology, 2007.

[15] A. Niskanen. *Radical Enhanced Atomic Layer Deposition of Metals and Oxides.* PhD thesis, University of Helsinki, 2006.

[16] S. C. Jain, M. Willander, J. Narayan, and R. Van Overstraeten. III-nitrides: Growth, characterization, and properties. *Journal of Applied Physics*, 87(3):965–1006, 2000.

[17] J. Toivonen. *Growth and properties of GaAsN structures.* PhD thesis, Helsinki University of Technology, 2003.

[18] S. Suihkonen. *Fabrication of InGaN Quantum Wells for LED Applications.* PhD thesis, Helsinki University of Technology, 2008.

[19] T. Lang. *Fabrication of Heteroepitaxial Templates for GaN-Based Optoelectronic Devices.* PhD thesis, Helsinki University of Technology, 2007.

[20] S. Sintonen. Superhilarakenteiden karakterisointi röntgendiffraktio- ja röntgenheijastusmenetelmillä. Master's thesis, Helsinki University of Technology, 2009.

[21] B. D. Cullity and S. R. Stock. *Elements of X-ray diffraction.* Prentice-Hall, Inc., New Jersey, 2001.

[22] D. K. Schroeder. *Semiconductor Material and Device Characterization.* IEEE Press, Piscataway, NJ, 2006.

Appendix A

Both X-ray reflectivity (XRR) and spectroscopic ellipsometer (SE) measurements were used to measure the thicknesses of the AlN films before and after thermal annealing. The refractive index of the films were also obtained by the SE measurements. The fitted and measured XRR and SE data is shown in figures A1 – A3 and A4 – A6, respectively.
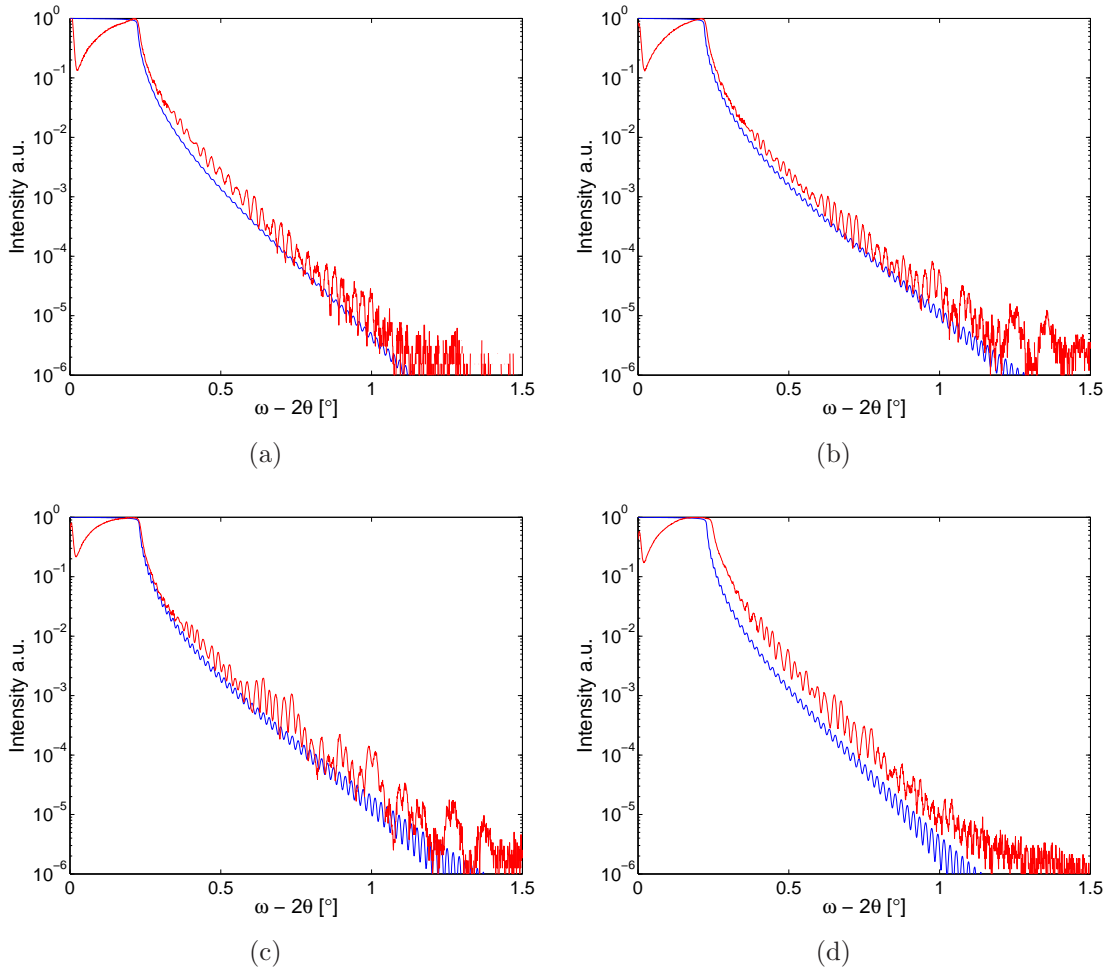

Figure A1: ω-2θ-scans and simulations of AlN films grown on (1 0 0)-oriented silicon (a) as deposited and annealed in RTP at temperature of (b) 600 °C, (c) 800 °C and (d) 1000 °C.
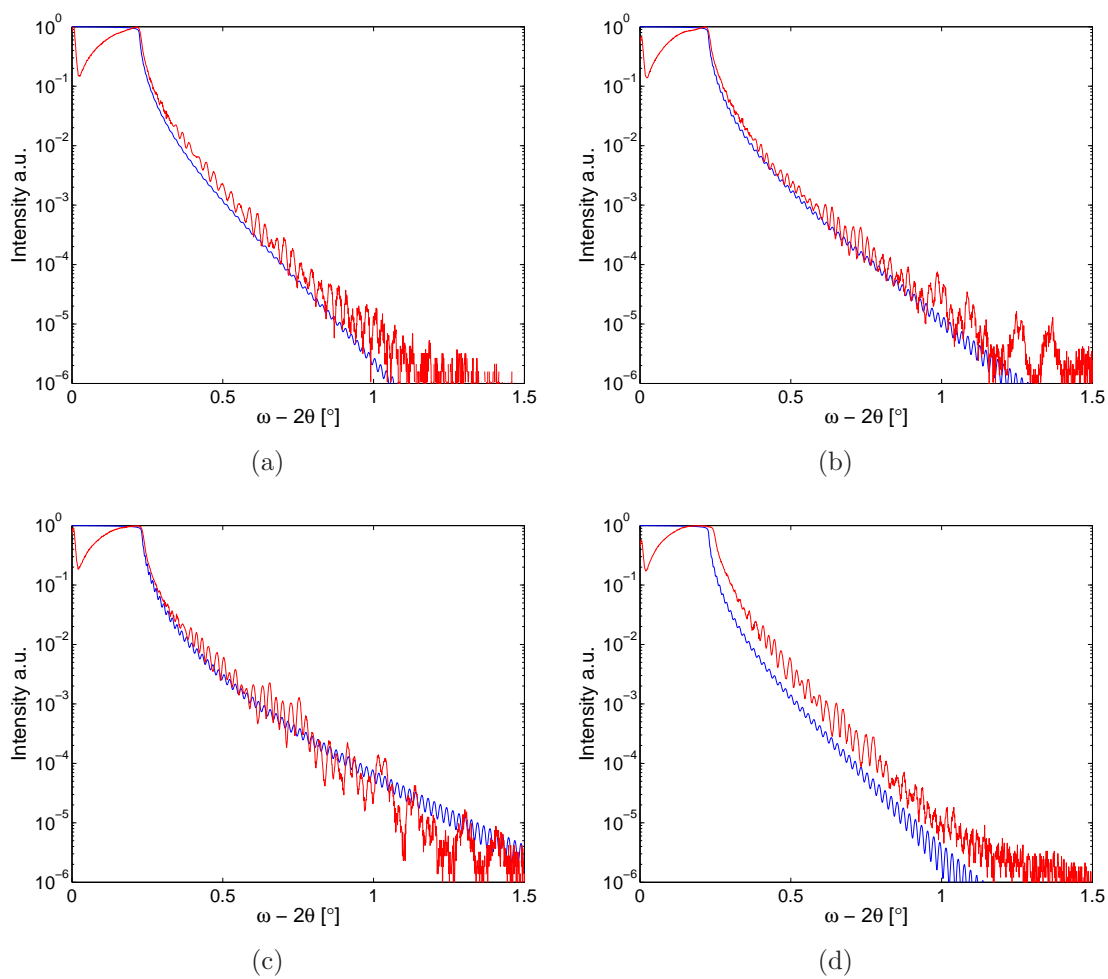
Figure A2: ω-2θ-scans and simulations of AlN films grown on (1 1 0)-oriented silicon (a) as deposited and annealed in RTP at temperature of (b) 600 °C, (c) 800 °C and (d) 1000 °C.
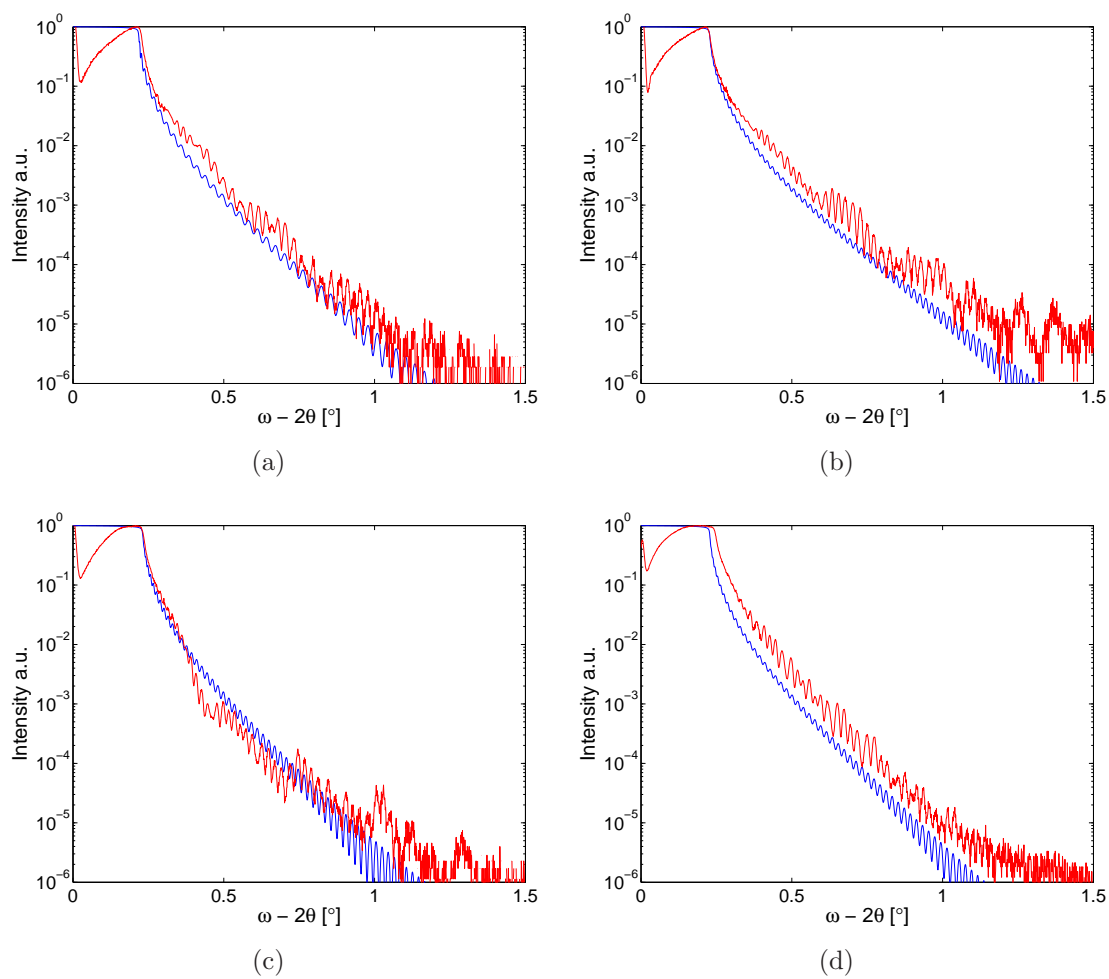
Figure A3: ω-2θ-scans and simulations of AlN films grown on (1 1 1)-oriented silicon (a) as deposited and annealed in RTP in temperature of (b) 600 °C, (c) 800 °C and (d) 1000 °C.
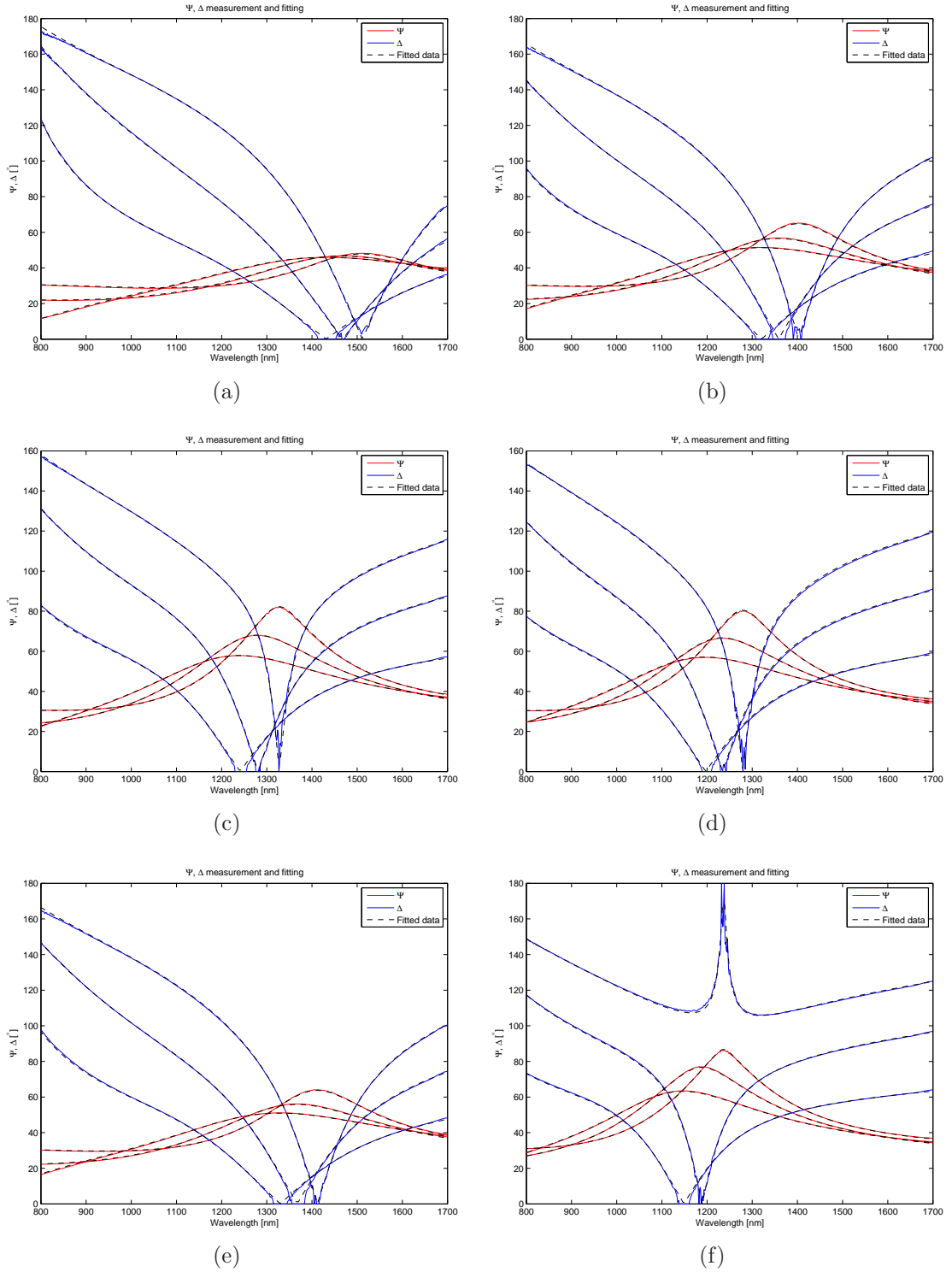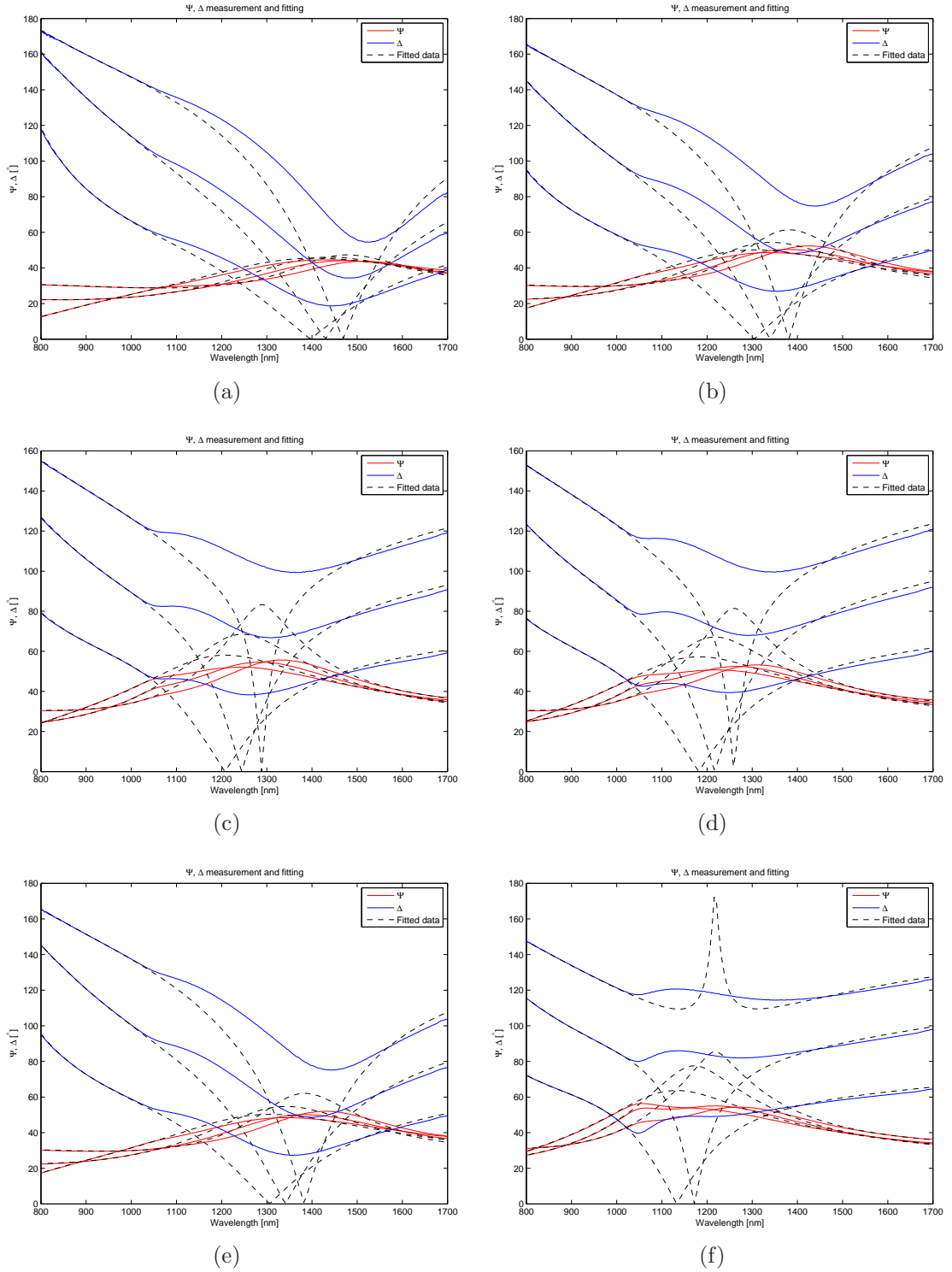
Figure A4: Ellipsometric measurement and simulation of AlN films grown on (1 0 0)-oriented silicon. Measured Ψ is drawn in red and Δ in blue. Fitted Ψ and Δ are shown in black dashed line. Film (a) as deposited, annealed in RTP at temperature of (b) 600, (c) 800 and (d) 1000 °C and in tube furnace at temperature of (e) 600 and (f) 1000 °C.
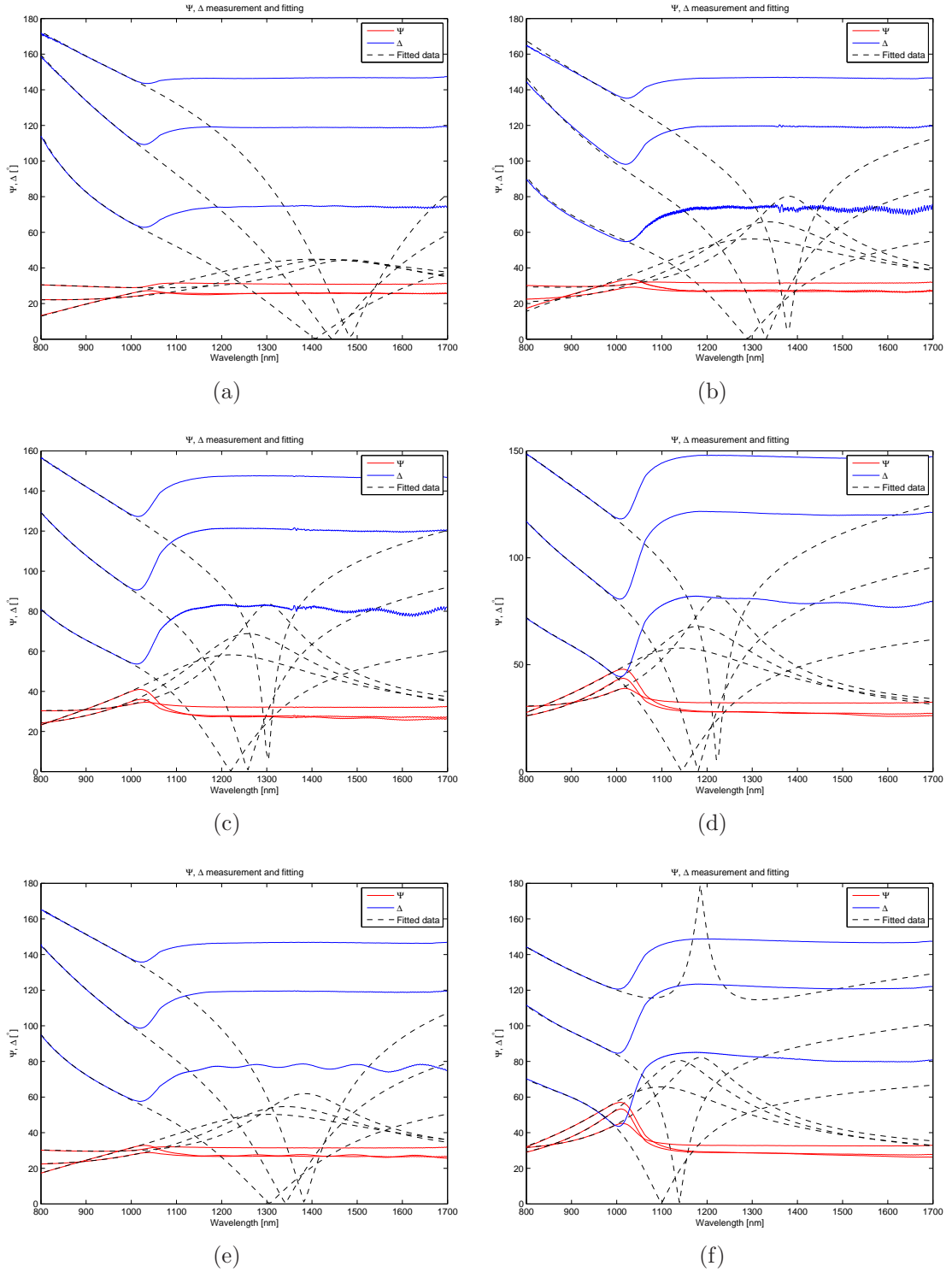
Figure A5: Ellipsometric measurement and simulation of AlN films grown on (1 1 0)-oriented silicon. Measured Ψ is drawn in red and Δ in blue. Fitted Ψ and Δ are shown in black dashed line. Film (a) as deposited, annealed in RTP at temperature of (b) 600, (c) 800 and (d)1000 °C and in tube furnace at temperature of (e) 600 and (f) 1000 °C.

Figure A6: Ellipsometric measurement and simulation of AlN films grown on (1 1 1)-oriented silicon. Measured Ψ is drawn in red and Δ in blue. Fitted Ψ and Δ are shown in black dashed line. Film (a) as deposited, annealed in RTP at temperature of (b) 600, (c) 800 and 1000 (d) °C and in tube furnace at temperature of (e) 600 and (f) 1000 °C.

Appendix B

AFM was used to obtain information about topography of AlN films films before and after thermal annealing. The films were shown to be smooth with the exception of the cracks formed during annealing. Only a few nanometers surface roughness can be seen in the AFM measurements. AFM measurements omitted from the results section are shown in figures B1 and B2.
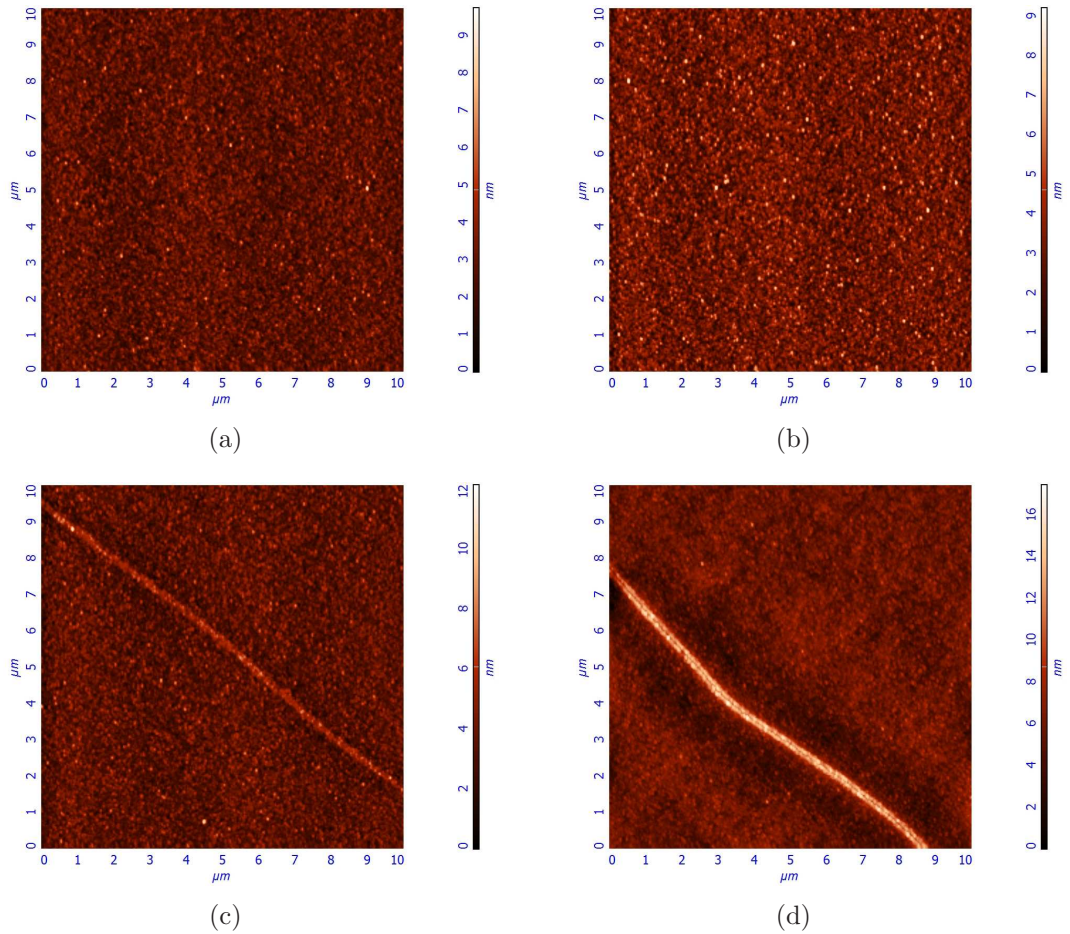

(a)   (b)

(c)   (d)

Figure B1: AFM images of AlN films grown on (1 0 0)-oriented silicon (a) as deposited and after annealing in RTP at temperature of (b) 600 °C, (c) 800 °C and (d) 1000 °C for 90 s. As can be seen the surface is very smooth, only a few nanometers of surface roughness. Thermal stress related cracks are seen in (c) and (d). However the cracks are most likely not seen properly due to tip convolution.
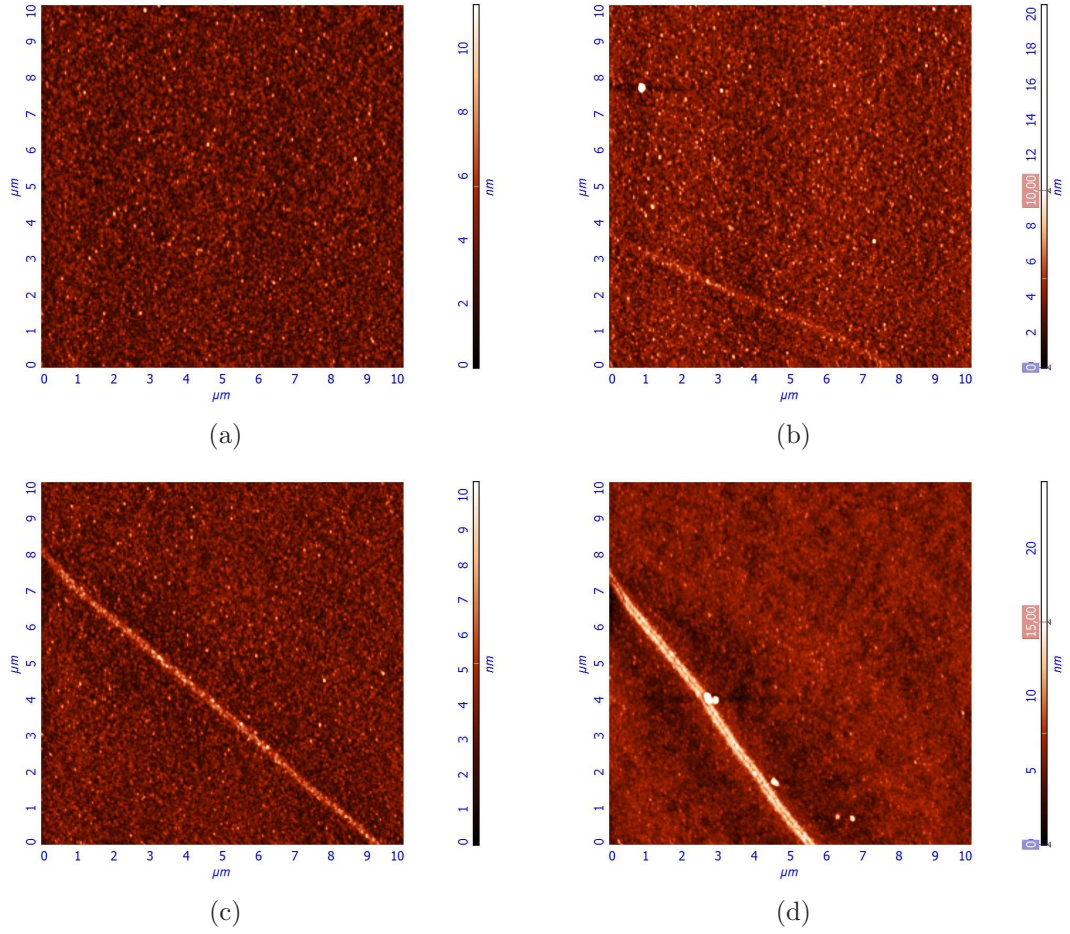
Figure B2: AFM images of AlN films grown on (1 1 0)-oriented silicon (a) as deposited and after annealing in RTP at temperature of (b) 600 °C, (c) 800 °C and (d) 1000 °C for 90 s. As can be seen the surface is very smooth, only a few nanometers of surface roughness. Thermal stress related cracks are seen in (b), (c) and (d). However the cracks are most likely not seen properly due to tip convolution. In (b) and (d) the coloration has been altered to obtain better contrast in images.

Appendix C

XRD measurements were used to study the crystal properties of the grown AlN films. No crystallinity of AlN films were found before or after annealing. Only difference in the measured samples the positions of the peaks originated from the silicon substrate. XRD measurements omitted from the results section is shown in figures C1 and C2.
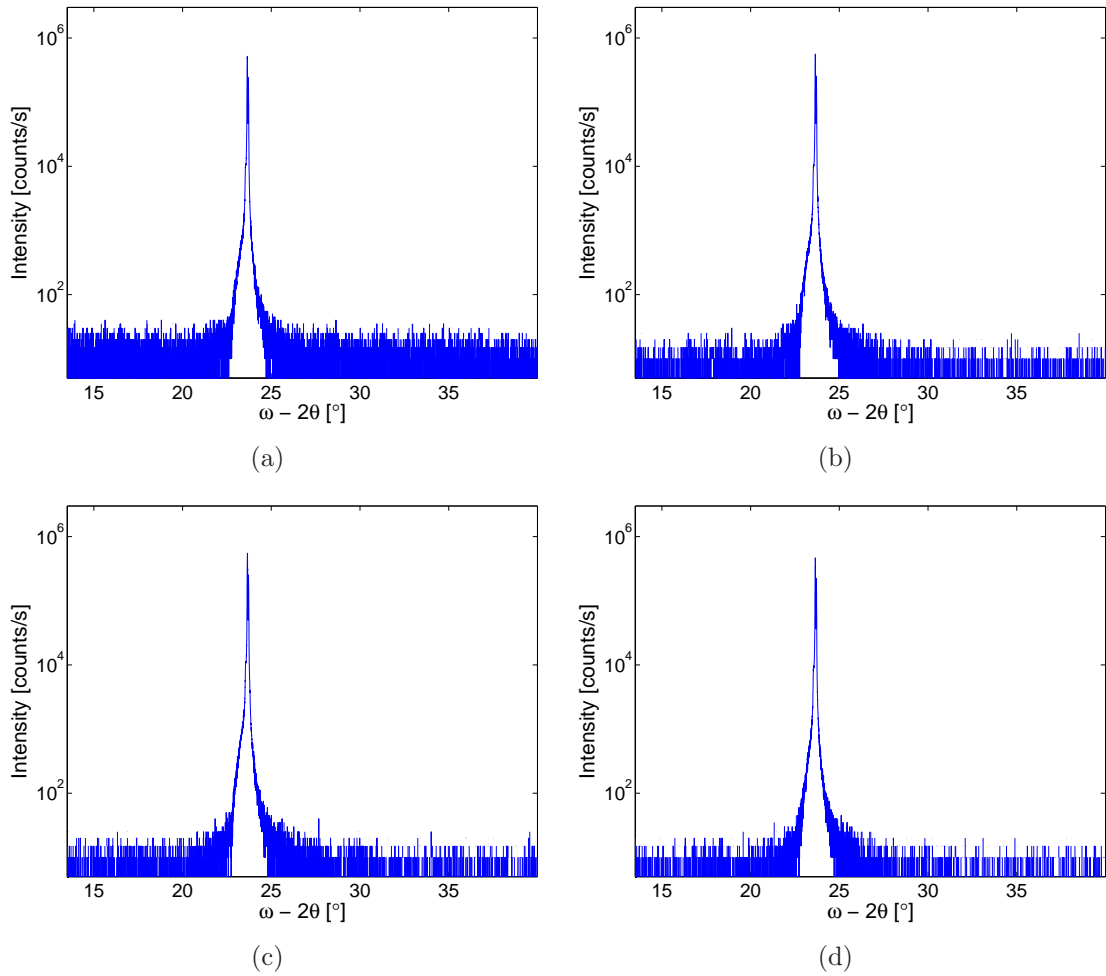

(a)

(b)

(c)

(d)

Figure C1: ω-2θ-scans of samples grown on (1 1 0)-oriented silicon substrate (a) as deposited and annealed at (b) 600 °C, (c) 800 °C and (d) 1000 °C. One diffraction peak was found in the measurements. The peak originates from the diffraction plane (2 2 0) of the silicon substrate.
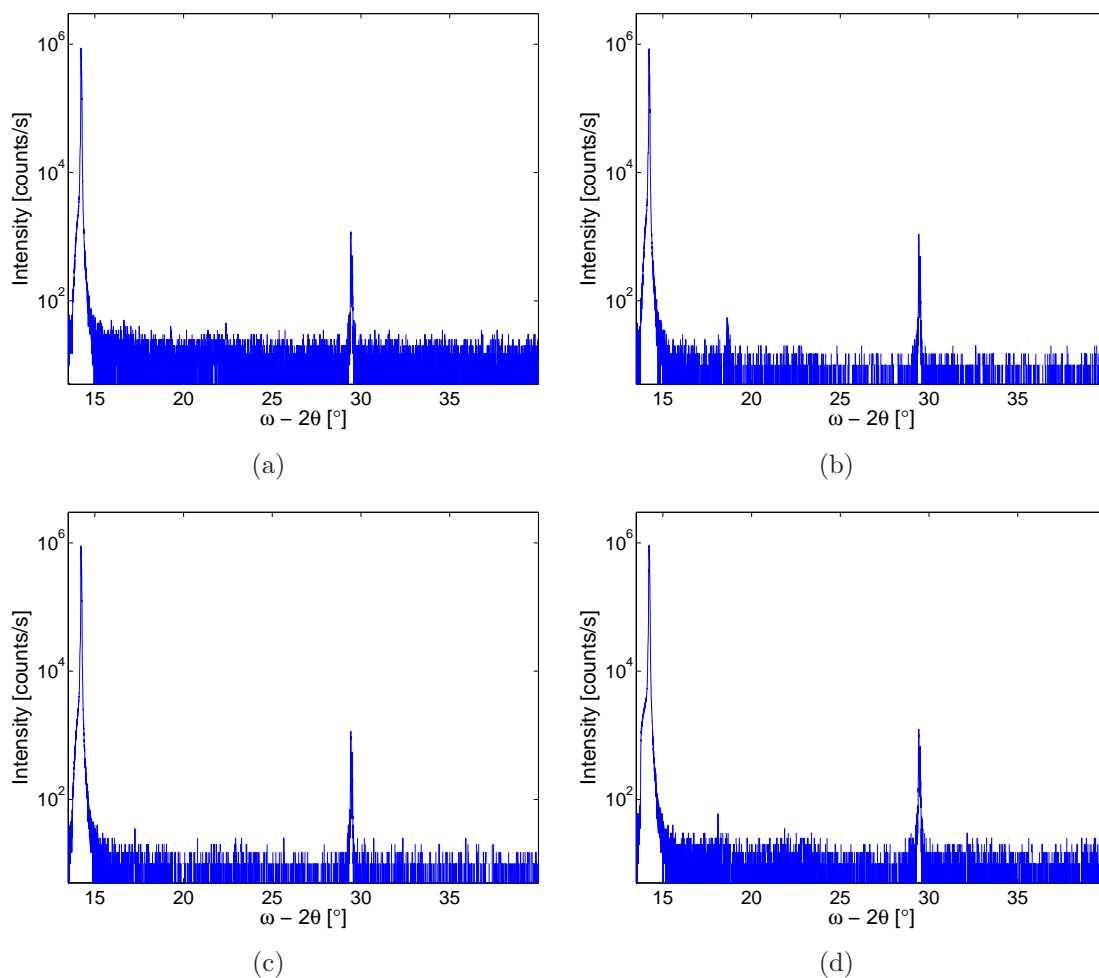
Figure C2: ω-2θ-scans of samples grown on (1 1 1)-oriented silicon substrate (a) as deposited and annealed at (b) 600 °C, (c) 800 °C and (d) 1000 °C. Two diffraction peaks were found in the measurements. These peaks originate from the diffraction planes (1 1 1) and (2 2 2) of the silicon substrate.